Synthesis of Catalytic Membrane Surface Composites for Remediating Azo Dyes in Solution

Synthesis of Catalytic Membrane Surface Composites for Remediating Azo Dyes in Solution

By

Alexander J. Sutherland, *B.Eng*

McMaster University

Department of Chemical Engineering

A thesis submitted to the School of Graduate Studies in partial fulfillment of the requirements of

McMaster University for the degree of Master of Applied Science

McMaster University

Master of Applied Science (2019)	McMaster University
(Chemical Engineering)	Hamilton, Ontario
Title:	Synthesis of Catalytic Membrane Surface Composites for Remediating Azo Dyes in Solution
Author:	Alexander J. Sutherland
Supervisor	Professor Charles-François de Lannoy
Number of Pages	xv, 97

Abstract

In the past 30 years zero-valent iron (ZVI) has become an increasingly popular reducing agent technology for remediating environmental contaminants prone to chemical degradation. Azo dyes and chlorinated organic compounds (COCs) are two classes of such contaminants, both of which include toxic compounds with known carcinogenic potential. ZVI has been successfully applied to the surfaces of permeable reactive barriers, as well as grown into nanoscale particles (nZVI) and applied in-situ to chemically reduce these contaminants into more environmentally benign compounds. However, the reactivity of ZVI and nZVI in these technologies is limited by their finite supply of electrons for facilitating chemical reduction, and the tendency of nZVI particles to homo-aggregate in solution and form colloids with reduced surface area to volume ratio, and thus reduced reactivity. The goal of this project was to combine reactive nanoparticle and membrane technologies to create an electro-catalytic permeable reactive barrier that overcomes the weaknesses of nZVI for the enhanced electrochemical filtration of azo dyes in solution. Specifically, nZVI was successfully grown and stabilized in a network of functionalized carbon nanotubes (CNTs) and deposited into an electrically conductive thin film on the surface of a polymeric microfiltration support membrane. Under a cathodic applied voltage, this thin film facilitated the direct reduction of the methyl orange (MO) azo dye in solution, and regenerated nZVI reactivity for enhanced electro-catalytic operation. The electro-catalytic performance of these nZVI-CNT membrane surface composites to remove MO was validated, modelled, and optimized in a batch system, as well as tested in a dead-end continuous flow cell system. In the batch experiments, systems with nZVI and a -2 V applied potential demonstrated synergistic enhancement of MO removal, which indicated the regeneration of nZVI reactivity and allowed for the complete removal of 0.25 mM MO batches within 2-3 hours. Partial least squares regression

(PLSR) modelling was used to determine the impact of each experimental parameter in the batch system and provided the means for an optimization leading to maximized MO removal. Finally, tests in a continuous system yielded rates of MO removal 1.6 times greater than those of the batch system in a single pass, and demonstrated ~87% molar removal of MO at fluxes of approximately 422 L/m^2h. The work herein lays the foundation for a promising technology that, if further developed, could be applied to remediate azo dyes and COCs in textile industry effluents and groundwater sites respectively.

Acknowledgments

Over the course of my undergraduate and graduate education at McMaster, I have been privileged with the opportunity to learn from an excellent cast of mentors. In the department of Chemical Engineering, I have benefitted immensely from the advice and teachings of professors such as Dr. Carlos Filipe, Dr. David Latulippe, Dr. Emily Cranston, and Dr. Jake Nease in my technical, professional, and personal development. I have been especially fortunate for the opportunity to work with my supervisor Dr. Charles-François de Lannoy. His dedication to learning, critical thinking, and improvement have been invaluable to my research and growth and continue to serve as a constant source of inspiration. I wish everyone could go through life with his passion and determination for pursuing new ideas and experiences, and it is these characteristics most of all that I hope to carry with me in all my future endeavours.

I would like to thank the members of the Latulippe Lab, the Kim lab, and the Canadian Center for Electron Microscopy for their assistance and generosity. It is with their help and willingness to share resources and expertise that I have been able to accomplish much of my work. I would also like to thank NSERC for providing the funding that has enabled me to take part in this adventure over the years.

I am also very grateful for the unceasingly hardworking administration within the Chemical Engineering Office. Michelle Whalen, Linda Ellis, and Kristina Trollip have helped me more times than I can remember, and always with the utmost patience and efficiency. I would also like to thank the brilliant technicians in our department: Paul Gatt, and Mike Clarke. Their expertise, creativity, and hard work were instrumental in developing the tools to overcome many of the challenging hurdles in my work.

I would like to express my gratitude and appreciation for the feedback, and support of my colleagues in the de Lannoy lab. Our collaborations throughout the years have been both productive and enjoyable. I would especially like to thank Amin Halali and Maria Ruiz-Caldas for welcoming me into the lab with open arms and for playing such a pivotal role in building my skillset as a researcher. I cherish all the time we spent together in the lab and feel as though we have shared the unique experience of defining its tone and culture.

These past few years in the Chemical Engineering department gave me the opportunity to develop relationships with people that I now count among my dearest friends. My experience at McMaster has been defined by golden moments brought forth by the sagely advice and wit of Daniel Osorio, the multi-faceted humour and colourful cynicism of Michael Kiriakou, and the sheer hilarity and boundless kindness of Taylor Stimpson. In particular, I feel that my friendships with Michael and Taylor have changed my life by re-forging my personality with new characteristics, which I can say with at least 37% confidence have altered me for the better. I cannot imagine a University experience without friends like these, who are solid as they come.

Lastly, I would like to thank my family from the bottom of my heart for all the love and support they've provided throughout the entirety of my academic career. Through TAing, I have realized that there is an art to offering someone just the right amount of help so that they might succeed on their own. In that, my parents – Carrie and Reid Sutherland – are Masters in their own right. Their care and guidance coupled with the encouragement and criticisms (which were of course, highly constructive) provided by my brothers Andrew and William have fundamentally set the stage for everything I have ever accomplished.

Table of Contents

Abstract ii

Acknowledgments iv

List of Abbreviations xi

List of Figures xii

List of Tables xv

Chapter 1 Introduction 1

Chapter 2 Background 5

2. 1 Chlorinated Organic Compounds 5

2.1.1 Organic Contamination in Soils and Groundwater 5

2.1.2 Difficulties in Remediating Chlorinated Organics in Soils and Groundwater 5

2.1.3 Current Treatment Strategies for COCs 6

2.2 Azo Dye Contamination 8

2.2.1 Classification and Usage of Azo Dyes 8

2.2.2 Threats Posed by Azo Dye Contamination 8

2.2.3 Current treatment Strategies for Azo Dyes 9

2.3 Membrane Technologies 10

2.3.1 Overview of Membrane Principles and Technologies 10

2.3.2 Challenges for Membrane Technologies 12

2.3.3 Modern Membrane Applications for Remediating COCs & Azo dyes 13

2.4 Electrically Conductive Membranes 14
2.4.1 Introduction to Conductive Membranes and Their Benefits 14
2.4.2 Graphitic Materials for Conductive Thin Film Surface Composites 15
2.5 Growing Reactive Nanoparticles 15
2.5.1 Zero Valent Iron 15
2.5.2 Reactive Nano Zero-Valent Iron Particles 16
2.5.3 Methods for nZVI Synthesis 16
2.5.4 Challenges Surrounding Nanoparticle Technologies 17
2.6 Stabilizing Reactive Nanoparticles 18
2.6.1 Surface coatings 18
2.6.2 Substrate-Supports 19
2.7 Objectives 20
Chapter 3 Proof of Concept Validation of the Electrocatalytic Properties of nZVI-CNT Surface Composites through Dye Removal in a Batch System 21
Abstract 21
3.1 Introduction 22
3.2 Materials and Methods 24
3.2.1 Materials 24
3.2.2 Catalytic Membrane Composite Preparation 24
3.2.3 Membrane Characterization 25

3.2.4 Electrochemical Batch Removal of Methyl Orange Dye 27
3.2.5 Cyclic Voltammetry 28
3.3 Results and Discussion 28
3.3.1 nZVI-CNT Membrane Composite Morphology 28
3.3.2 Catalytic Membrane Conductivity and Iron Content 29
3.3.3 MO Batch Removal Performance of Catalytic Membranes 31
3.4 Conclusions 34
Chapter 4 Application of Catalytic Membranes in a Continuous Dead-End Flow System 35
Abstract 35
4.1 Introduction 36
4.2 Materials and Methods 37
4.2.1 Materials 37
4.2.2 Catalytic Membrane Composite Preparation 38
4.2.3 Membrane Characterization 38
4.2.4 Membrane Flow Characterization 39
4.2.5 Continuous Electrochemical Removal of Methyl Orange Dye 39
4.2.6 Contact Angle Experiments 41
4.3 Results and Discussion 41
4.3.1 nZVI-CNT Membrane Composite Morphology 41
4.3.2 Catalytic Membrane Flux and Permeability 42

4.3.3 Continuous Removal of MO Using Catalytic Membranes 43
4.4 Conclusions 50
Chapter 5 Statistical Modelling and Optimization of the Batch Removal Performance of Catalytic Membranes using Latent Variable Methods 51
Abstract 51
5.1 Introduction 52
5.2 Materials and Methods 52
5.2.1 Materials 52
5.2.2 Catalytic Membrane Composite Fabrication with Varying Parameters 53
5.2.3 Methyl Orange Batch Removal Experiments 53
5.2.4 Modelling Batch Removal Over Time Using PLSR 55
5.2.5 Using PLSR to Predict Optimal Batch Removal Performance 57
5.2.6 Projecting Batch Removal Performance Using Auto-Regression PLS 59
5.3 Results & Discussion 60
5.3.1 Modelling Batch Removal Over Time Using PLS 60
5.3.2 Using PLS to Predict Optimal Batch Removal Performance 64
5.3.3 Projecting Batch Removal Performance Using Auto-Regression PLS 66
5.4 Conclusions and Future Work 69
Chapter 6 Conclusions and Future Work 70
6.1 Conclusions 70

6.2 Future Work and Recommendations 73

Appendix A: Supporting Information 75

Description of the custom continuous dead-end flow cell 77

Measurement error in continuous experiments examining the effect of the mid-test application of voltage 77

Appendix B: References 80

List of Abbreviations

ARPLS	Auto-regression partial least squares
CMC	Carboxymethyl cellulose
CNT	Carbon nanotube
COC	Chlorinated organic compound
COD	Chemical Oxygen Demand
CV	Cyclic Voltammetry
DIW	Deionized Water
DLVO	Derjaguin Landau Verwey Overbeek
DNAPL	Dense non-aqueous phase liquid
DO	Deoxygenated
EDS	Energy-dispersive x-ray spectroscopy
EPS	Extracellular polymeric substance
GO	Graphene oxide
ICP-OES	Inductively coupled plasma optical emission spectroscopy
MF	Microfiltration
MO	Methyl Orange
NF	Nanofiltration
nZVI	Nano zero-valent iron
PCB	Polychlorinated biphenyl
PCE	Perchloroethene
PES	Polyether sulfone
PLSR	Partial least squares regression
PRB	Permeable reactive barrier
PVA	Polyvinyl alcohol
PVDF	polyvinylidene fluoride
RO	Reverse osmosis
ROS	Reactive oxygen species
SEM	Scanning electron microscopy
TCE	Trichloroethylene
TEM	Transmission electron microscopy
UF	Ultrafiltration
VOC	Volatile organic compound
ZVI	Zero-valent iron

List of Figures

Figure 2.1. The relative size of common contaminants, and the membrane separation pore size regimes used to separate them. Reproduced from [74]..... 11

Figure 3.1. Mechanisms for the degradation of azo dyes by a) direct reduction and c) ROS mediated reduction, and mechanisms for the degradation of COCs by b) direct reduction and d) ROS mediated reduction. 22

Figure 3.2. The experimental setup for testing nZVI-CNTs performance in removing MO in solution under an applied voltage. 27

Figure 3.3. TEM-EDS images showing an nZVI-CNT mixture (left) and its main elemental composition in terms of carbon (middle) and iron (right). 29

Figure 3.4. Left: Conductivity results from 4-point probe measurements on nZVI-CNT and CNT membrane composites, and right: Cyclic voltammetry on the batch removal system using an nZVI-CNT cathode, with a grey dotted line shown to outline the MO reduction peak. 29

Figure 3.5. Results for batch removal of MO using nZVI-CNT cathodes (grey) and CNT cathodes (black), operating at -2V (squares) or with no applied voltage (circles). Error bars represent the 95% confidence interval. 32

Figure 4.1. a) A visual and b) a schematic of the continuous dead-end flow system used to test the catalytic membrane's performance in electrochemically degrading MO. 40

Figure 4.2. An SEM image of an nZVI-CNT membrane cross section at 5,000x magnification, showing both the thin film surface composite and the PES support membrane beneath it. 41

Figure 4.3. Pure water flux measurements for 0.45 μm pore size PES membranes (grey) and 0.45 μm pore size PES membranes with 4 mg of nZVI-CNT surface composites at 20-80 psi pressures. 42

Figure 4.4. MO mole % Removed (orange) and Average Flux (blue) for dead-end continuous flow cell tests at 40 psi with various membrane surface composite cathode types and applied voltages. Error bars represent the 95% confidence interval on each set of triplicate tests. 43

Figure 4.5. Removal rates for dead-end continuous flow cell tests with various membrane surface composite cathode types and applied voltages. Error bars represent the standard deviation across three triplicates. 45

Figure 4.6. MO Mole % Removed (orange) and Average Flux (blue) for a dead-end continuous flow cell tests at 40 psi using an nZVI-CNT membrane composite cathode, in which a step change in applied voltage of 0 V to -2 V is made after 30 minutes elapsed. 46

Figure 5.1. A schematic of the MO batch removal experiments, in which voltage is supplied to the surface of the composite cathode, and a graphite strip anode. 54

Figure 5.2. A structural visualization of the matrix blocks used in a PLSR model. 56

Figure 5.3. Cumulative $R2$ (gray), and cumulative $Q2$ (black) attained by a PLSR model with the addition of a first and second component fit to the MO batch removal experiment data. 60

Figure 5.4. Input weights $W1$ (gray) and output weights $C1$ (black) for the first component of a PLS model fit to the MO batch removal experiment data. 61

Figure 5.5. Observed (black circles) vs. predicted (white circles) values for MO removal at optimal experimental parameters, as determined by the PLS model. The range of other experimental tests is shown for comparison. 66

Figure 5.6. An observed (black circles) vs. predicted (white circles) plot used to validate the accuracy of the ARPLS model created on the optimum RO removal timeseries data. 67

Figure 5.7. A timeseries plot of observed experimental values (black circles) for MO removal using optimal parameters, extended using predictions made by the ARPLS model (white circles).

Error bars on the predictions come from 95% prediction intervals, and the red represent the cumulative prediction intervals. 68

List of Tables

Table 2.1. nZVI surface coating types with examples [7], [28], [112]–[119], [104]–[111]. 19

Table 4.1 Structure and results of a design of experiments investigating the effects of feed concentration and pressure on the flux and mole % removal of continuous tests using a system operating at -2 V with an nZVI-CNT cathode, as well as the results of triplicate tests previously discussed for comparison (blue). 49

Table 5.1. Experimental parameters for electrochemical batch removal tests using catalytic nZVI-CNT membrane surface composites. 55

Table 5.2. Input and output variables used to construct a PLSR Model on the batch removal system. 55

Table 5.3. Definitions, dimensions, and indices for the matrix blocks in a PLSR model. Note that W', C', and P' denote the transposes of the W, C, and P matrices respectively. 57

Table 5.4. Input decision variable constraints for optimizing the batch removal of MO at 60 min. 58

Table 5.5. Results for the predicted and observed values of optimum MO removal. The decision variables at the optimum and the constraints they are subject to are also shown. 65

Table S.1. Data for 41 batch tests used to construct the PLSR model discussed in Chapter 5. Samples are coded according to the contents of their surface composites with the following convention: “CT” = nZVI-CNT, “T” = CNT, “S” = None. 79

Chapter 1

Introduction

The remediation of water sources polluted by organic contaminants presents a significant challenge for modern wastewater treatment [1], [2], [3]. Within the category of organic pollutants, chlorinated organic compounds (COCs) and azo dyes represent considerable threat, due to their toxicity, carcinogenic potential [1], [4]–[6], and widespread contamination of groundwater sites and textile industry effluents respectively [7], [8]. Furthermore, both types of compounds have proven highly resistant to conventional wastewater treatment practices, and biodegradation in aquatic ecosystems [1], [5].

Membrane technologies have become ubiquitous over the past few decades and are now the method of choice for accomplishing a wide variety of wastewater separations [9]–[14]. Among the types of conventional membranes, reverse osmosis (RO) have been applied to successfully remove COCs and azo dyes from the environments they contaminate [15], [16]. While RO membranes demand large pressure gradients (and thus significant degree of energy) to conduct a separation, membranes with larger pores and less demanding energy constraints cannot be used due to the small size of the aforementioned organic contaminants. The buildup of biofouling and scaling on the surface of these membranes increases the transmembrane pressure (TMP) and thus energy requirements to conduct a given separation [14], [16]–[18]. The accumulation of rejected contaminants and other ions in solution can also damage the membrane through concentration polarization, and further increase the TMP requirements through a buildup of osmotic pressure. In light of these limitations and costly energy requirements, methods other than RO have been explored for remediating azo dyes and COCs in wastewaters. The current industrially favoured

solutions for remediating these contaminants are advanced oxidation processes in azo dye textile industry effluents [19], and the use of chemical reductants in groundwaters and soils contaminated with COCs [20]–[23].

Metallic iron possessing an oxidation state of zero, otherwise known as zero-valent iron (Fe^0, or ZVI), is a chemical reductant capable of remediating both azo dyes and COCs in solution [22], [24]–[28]. ZVI accomplishes the remediation of these compounds by degrading the azo linkages and chloride bonds of azo dyes and COCs respectively [20], [26], [29]. ZVI has become a viable technology for organic remediation due to its high reactivity, low toxicity, low cost, and natural abundance [21], [27], [30]–[32].

The performance of ZVI can be improved by fabricating this material in nano-scale particles. Doing so results in nano zero-valent iron (nZVI) which possesses enhanced reactivity due to its vastly increased surface area to volume ratio (>1000 times) [22], [26], [29], [33]–[36]. However, nZVI's reactivity is limited by two main challenges. The first of these challenges is the aggregation of nZVI particles into colloids, which significantly decreases their collective surface area to volume ratio, and thus their reactivity [26], [31], [32], [34], [37], [38]. Secondly, while nZVI is an effective reducing agent, it is not selective in the compounds it reacts with. As such, much of nZVI's reactivity can be wasted reducing compounds in solution other than the target contaminants [22]. Regardless of whether nZVI spends its reactivity on target contaminants or other scavenging compounds in solution, nanoparticle oxidation inevitably limits nZVI's ability to operate in a continuous setting.

Graphitic materials such as carbon nanotubes (CNTs) may offer a solution to the challenges facing both membrane technologies and nZVI in the face of remediating azo dyes and COCs. Prior work has shown that CNTs can be used to construct electrically conductive, permeable thin film

composites on the surface of polymeric support membranes [39]. With an applied voltage, these composites demonstrate remarkable resistance to biofouling [14], [39]–[45]. Additionally, functionalized CNT networks have also been used as a substrate for stabilizing metal nanoparticles to prevent their homoaggregation [31], [46], [47]. CNT networks accomplish nanoparticle stabilization by sterically segregating them across their large surface areas, and by electrostatically stabilizing the positive charge of their metal ion precursors with negatively charged functional groups [31], [46]–[50]. Furthermore, CNT thin films have shown promise as electrodes for effectively degrading azo dyes through electrochemical reaction under applied electric potentials [51], [52].

The objective of this thesis was to produce electrically conductive CNT membrane surface composites with embedded nZVI, capable of electrochemically removing azo dyes in solution under a negative applied potential. In this system, polymeric membranes with pore sizes in the microfiltration regime were used simply as a porous support for an nZVI-CNT nanocomposite thin film. Rather than facilitating contaminant separation based on size exclusion or solution diffusion mechanisms, these nZVI-CNT composite membranes serve as reactive barriers with which to electrochemically degrade contaminants under an applied voltage. While COCs remain an important and prevalent hazard to the environment, azo dyes were studied exclusively in this project because they are substantially safer to work with and their concentration change is easier to evaluate. The contaminant removal techniques developed herein are applicable to both azo dyes as well as COCs.

We investigated whether it was possible to channel electrons to the embedded nZVI particles via the conductive CNT network and continuously regenerate their reactivity for the enhanced electrocatalytic contaminant degradation. A simple batch system was devised to

accomplish this task, in which membrane surface composites were employed as a cathode opposite a graphite foil anode in a stirred azo dye solution.

The results of the simple batch experiments, as well as other tests with varying experimental parameters were analyzed using Partial Least Squares Regression (PLSR) modelling. The models developed provided 1) insight into the impact of each experimental parameter on contaminant removal, 2) the opportunity to determine the optimal set of system parameters for achieving maximum contaminant removal, and 3) an extended timeseries projection of contaminant removal at that optimum.

Finally, the nZVI-CNT composite membrane cathode/graphite anode batch system was redesigned into a dead-end flow cell to evaluate this technology's performance in the continuous removal of an azo dye feed. Contaminant removal and transmembrane flux were used in combination as metrics to assess this performance, and design of experiments was conducted to assess the impacts of feed concentration, and feed pressure on contaminant removal. The observed success in continuously remediating an azo dye contaminant with nZVI CNT surface composite membranes shows promise for applying this technology as a final excess dye removal step in textile industry effluent wastewater treatment processes.

Chapter 2

Background

2. 1 Chlorinated Organic Compounds

2.1.1 Organic Contamination in Soils and Groundwater

The organic contamination of soils and groundwater systems poses one of the largest challenges in modern environmental remediation [1], [2]. Volatile organic compounds (VOCs), chlorinated organic solvents, pesticides, and other chlorinated aromatics all pose significant threat to human health through the soils and groundwaters they contaminate [1], [2]. Among these types of organic pollutants, chlorinated solvents are the most common [21], [53]. Studies have shown that many of these compounds become hazardous to human health after being processed in the liver [1]. Chlorinated organic compounds (COCs) such as trichloroethylene (TCE), perchloroethene (PCE), and polychlorinated biphenyls (PCBs), are found in thousands of soil and groundwater sites in North America and Europe alone [38]. Such contamination is the by-product of various industrial activities including pesticide run-off, discharge from metal degreasing, dry cleaning, and chemical spills [1], [23], [33], [38].

2.1.2 Difficulties in Remediating Chlorinated Organics in Soils and Groundwater

Without even considering the mechanisms of contaminant remediation, the treatment of soils and groundwater remains a complex challenge due to the wide variety of organic pollutants and the sites in which they are found. Many chlorinated solvents are heavier than water (including TCE, $\rho_{TCE} = 1.46$ g/mL) and therefore permeate downward through groundwater systems and form plumes of dense non-aqueous phase liquid (DNAPL) [1]. In 2005 the United States Environmental Protection Agency estimated that the number of groundwater sites contaminated

with DNAPLs in the US ranges from 15 000 to 20 000 [7]. DNAPLs are capable of migrating vertically and laterally through aquifer systems, and leave a trail of contamination in their wake [1]. The ability of these contaminants to spread through groundwaters raises the difficulty of developing methods that efficiently capture and remove them from solution.

Furthermore traditional wastewater treatment techniques such as coagulation, sedimentation, filtration, etc. have proved ineffective for reducing the concentrations of TCE below hazardous levels [1]. Due to its chemical structure, TCE is not easily biodegraded or otherwise transformed through chemical reactions into environmentally benign compounds [1].

2.1.3 Current Treatment Strategies for COCs

2.1.3.1 Ex-situ Treatment

Ex-situ remediation technologies are often referred to as "pump-and-treat" methods, because they involve the removal of polluted groundwaters and soils from their site to remediate them with technologies on the surface. Air stripping is an ex-situ technique that takes advantage of the low Henry's constant and solubility of VOCs, and uses a counter-current stream of air to remove those contaminants from the liquid phase and into the gas (air) phase [1]. However, concentration targets for TCE removal often require an infeasible flow rate of air to obtain. Furthermore, in this method the contaminant compound is simply transferred into another phase, rather than being degraded or otherwise transformed into something less harmful [1].

2.1.3.2 In-situ Treatment

Soil Venting relies on the same mechanism as air stripping, but forces air into the soil in-situ. Once the air streams have stripped contaminants from the groundwater, they are directed to wells where the COCs can be collected or released to the atmosphere [1][2]. This technology faces

the same limitations as air stripping, with the added challenges that it is more expensive to build and operate in-situ.

Permeable reactive barriers (PRBs) are loose obstacles to flow possessing reactive metallic iron in its zero-valent state. Zero-valent iron (ZVI) is capable of degrading COCs through a reduction mechanism in which the chloride bond is broken down (also known as dechlorination) [20]–[23]. PRBs are an attractive technology because ZVI is effective at reducing contaminants and because once installed PRBs require no energy to operate. However, PRBs rely on the transport of contaminants passed their surface, and can take a long time to accomplish the remediation of aquifers that have COC contamination spread out over large distances [7]. Furthermore, since the ZVI lining a PRB permanently uses up its reactivity on contaminants and scavenging compounds alike, PRBs are single use. Add in the high capital costs for installation, and PRBs quickly become a very expensive option [20].

The targeted injection of chemical reductants is another method for remediating soils in-situ [23]. Electron-donating reduced metal species such as Fe^0, Fe^{2+}, Fe_3O_4, FeS, and FeS_2 are capable of degrading chlorinated organic compounds by chemical reduction [23]. Highly reactive nanoscale iron particles can be stabilized in a clay matrix [20], [54], [55] and mixed with contaminated soils for their in-situ remediation. At least nine full scale plants have been developed to treat COC contaminated soils this way, but the technology is limited to applications less than 50 feet deep where the soil can be easily mixed [20].

2.2 Azo Dye Contamination

2.2.1 Classification and Usage of Azo Dyes

Dyes exhibit a wide range of structural diversity and are commonly classified by their solubility in water. Acid, basic, direct, metal-complex, mordant, and reactive dyes are soluble in water, while the insoluble class is made up of azoic, disperse sulfur, and vat dyes [8]. Azo dyes are defined as aromatic compounds possessing one or more -N=N- azo linkages [3]. The azo linkage is a chromophoric chemical group, and is largely responsible for giving the dye its colour [3]. The dye's colour is further dependent on what kinds of auxochromic substituents it has on the aryl rings in its chemical structure [56]. Over 100 000 types of commercial dyes exist, and global dye productions are estimated to be between $7 \times 10^5 – 1 \times 10^6$ tons per year. Azo dyes constitute the large class of commercial synthetic dye [3], and account for approximately 70% of the dyes used by humans as a whole [8].

2.2.2 Threats Posed by Azo Dye Contamination

Azo dyes are commonly used in the textile, pharmaceutical, and printing industries [4], [29], [35], and up to 10-15% of azo dyes used in these applications are discharged to aquatic environments [8]. Thus, incorporating the production data provided in the previous subsection (2.2.1), approximately 77,000 tons of azo dyes are discharged to aquatic environments per year. Azo dyes and the compounds they are transformed into by the human body have been found to be toxic, and in many cases carcinogenic [4], [5], [6]. Regulations set by the European Union Water Framework Directive and the Department for Environmental Food and Rural Affairs are combating this pollution by tightening regulations on textile industry effluents [57].

2.2.3 Current treatment Strategies for Azo Dyes

Azo dyes and other synthetic dyes are resistant to photolysis, able to withstand high temperatures, and are not easily biodegraded [5]. These attributes make the removal of azo dyes from water difficult. Instead of relying on conventional wastewater treatment techniques such as filtration, sedimentation, and aerobic/anaerobic digestion, azo dyes are currently removed from industrial wastewaters through advanced oxidation processes, adsorption, electrochemical reaction, and advanced biodegradation. The most industrially used type of these methods are advanced oxidation processes, which remove dyes by oxidizing the azo linkages and the aryl rings found in their structures [19]. These strong oxidants are typically compounds that can produce hydroxyl radicals in solution, such as O_3 and H_2O_2 [3]. The oxidative removal of azo dyes can be improved through increasing hydroxyl radical concentrations using Fenton's reagent (Fe^{3+}/H_2O_2) and/or applying ultraviolet light to promote degradation by photolysis [58]. However, the high cost of these oxidizing agents is a limiting factor for conducting large scale dye remediation [59].

Instead of applying pre-synthesized oxidizing agents to remediate azo dyes, electrochemical cells can be used to generate strong oxidants that degrade dyes in solution. Electrochemical systems can achieve dye removal in a variety of other ways, including by direct reduction at a cathode, electrochemical oxidation, electrocoagulation, and electro-Fenton reactions, just to name a few [51], [60]–[63]. The electrodes in these systems are made from a diverse array of conductive materials, with metals like platinum and titanium, and graphitic materials such as graphite, graphene, and carbon nanotubes [51], [52], [64]. Microbial fuel cells build upon these systems by using microbes that catalyze dye oxidation at the anode, and reduction at the cathode [61], [65].

Azo dye adsorption using activated carbon, peat, wood chips, etc. as sorbents presents an alternative technology and removal mechanism, but also struggles due to the economic cost and the difficulty of sorbent regeneration [59], [66].

2.3 Membrane Technologies

2.3.1 Overview of Membrane Principles and Technologies

Membrane technologies can be broadly described as semi-permeable barriers that separate a pressurized contaminated feed stream into two parts: a retentate stream rejected by the membrane, and a permeate stream permitted by the membrane. Over the past few decades, membrane separation technologies have risen to prominence in both the academic and industrial sectors for their success in treating wastewaters from a variety of sources, as well as for the opportunities they present for process intensification [9]–[14]. Their applications include, but are not limited to, municipal, industrial, and textile wastewater treatment, as well as desalination, distillation, food processing, gas separations, and fuel cells [44], [67]–[73].

Conventional membranes achieve the removal of contaminants in a feed under an applied pressure by the mechanism of size exclusion; denying the passage of contaminants too large to travel through the membrane's pores [13], [71]. Size exclusion is the most common mechanism for conducting membrane separations, and as such, membranes are often classified based on the size of their pores. In order of decreasing size, these categories are microfiltration (MF), ultrafiltration (UF), nanofiltration (NF), and reverse osmosis (RO) [71]. Importantly, reverse osmosis membranes stand apart from these other categories in that they do not possess pores for separation through size exclusion, and instead rely on the mechanism of solution diffusion [12], [71]. Figure 2.1 below shows a variety of common waterborne contaminants, as well as the general pore sizes of the different conventional membrane classifications [74].

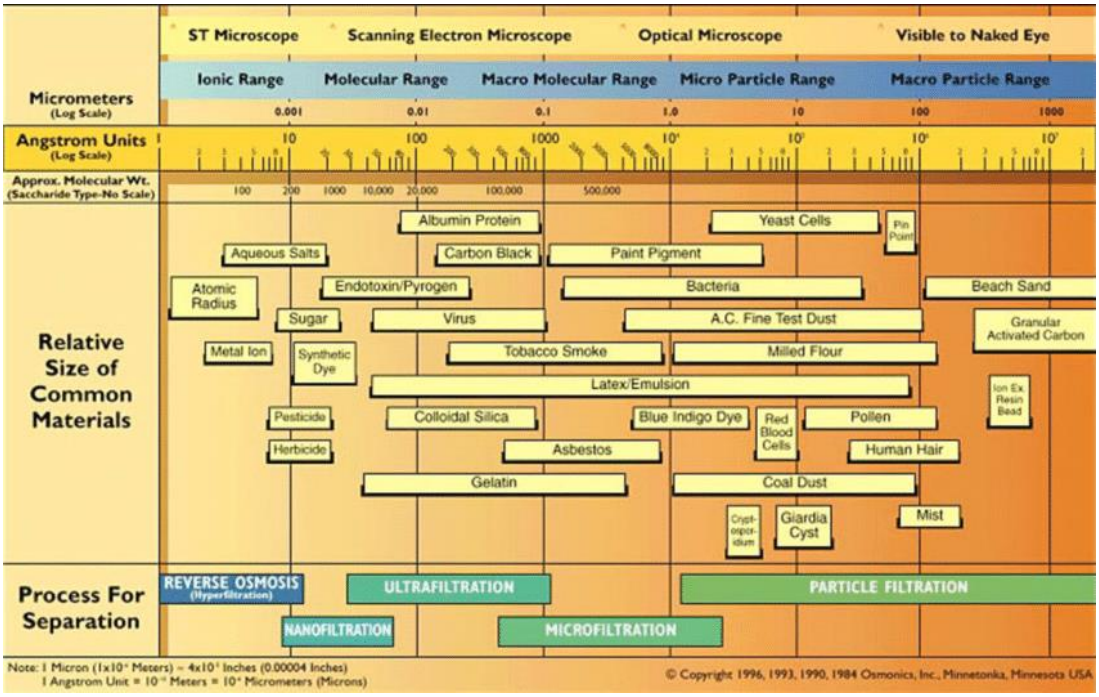

Figure 2.1. The relative size of common contaminants, and the membrane separation pore size regimes used to separate them. Reproduced from [74].

While conventional size exclusion remains the most common separation mechanism utilized in membrane technologies, a wide variety of other bases for membrane selectivity exists in industry and academia. For instance, membranes used in gas separations are non-porous and selective based on the diffusivity of the feed particles in the membrane material [72], while membranes for ion exchange conduct separation based on charge [75].

Membranes are typically made of polymers such as polyvinyl alcohol (PVA), polyvinylidene fluoride (PVDF), polyether sulfone (PES), as well as biopolymers like cellulose nitrate and cellulose acetate [71], [76]. However, the material used to construct a membrane can vary widely depending on the separation it is intended for.

2.3.2 Challenges for Membrane Technologies

While membranes have been proven to be highly effective, economically favourable, and customizable in achieving a variety of separations, they are universally limited by the problem of fouling. Fouling is a buildup of material on or inside the membrane's matrix that obstructs flow through its pores. This obstruction leads to decreased flux and permeability for constant TMPs [14], [71], [73], [77]. Depending on the system and the compounds present in the feed, fouling can be either reversible (by cleaning with methods such as back-washing) or non-reversible. Foulants can be divided into four main types: micro-biological organisms, organics, inorganics, and particulates [14].

Biofouling is when bacteria in solution cause the formation of one or more layers of biofilm on the membrane's surface [14], [78], [79] and is generally considered the most ubiquitous type of fouling in membrane applications. Though the process of biofouling has been found to have many stages [78], it can be generally divided into following two steps: 1) the irreversible attachment of bacteria to a membrane's surface and 2) the generation of an extracellular polymeric substance (EPS) by those bacteria that covers the surface [80]. Biofouling is further problematic because the EPS layer formed is resistant to many common membrane cleaning procedures [80].

Particulate and colloidal fouling involves the buildup of organic or inorganic compounds between 0.001 μm and 1 μm in size [14]. Depending on the size of the solids involved, colloids can either cause blockages in the pores themselves or merely develop a layer of material on the membrane surface [73], [81], [82]. The rate and extent of colloidal fouling is highly dependent on the shear rate, bulk concentration, and particle size of the feed solution [83].

Organic foulants can be either dissolved or colloids, but share the commonality of attaching to the membrane's surface through adsorption [14]. While inorganic foulants also refer to dissolved components, these compounds are metals that precipitate onto the surface of the membrane due to either oxidation or change in pH [14], [84], [85]. This phenomenon is also known as scaling.

Broadly speaking, the rate and extent of fouling is highly dependent on the operating conditions, as well as the bulk concentration, and particle size of the feed solution [83].

2.3.3 Modern Membrane Applications for Remediating COCs & Azo dyes

Conventional reverse osmosis membranes have been used to completely remove chlorinated solvents [15] and dyes [16] from wastewater effluents but are limited by a variety of problematic factors. These factors include high energy costs required to drive the separation (particularly in high-salinity solutions that result in large osmotic pressures), membrane damage due to concentration polarization, and biofouling that is incurred without expensive pre-treatment steps [16]–[18].

Membrane technologies have also been utilized for removing COCs from wastewaters through pertraction. Pertraction is a method in which a contaminant is transferred through liquid-liquid extraction across a membrane barrier from a flow of contaminated wastewater feed to a solvent flowing in countercurrent [86]–[88]. A good solvent for this technique is one that has high affinity for the contaminant, very low solubility in water, is non-toxic, and is easily reused [86]. The main costs associated with pertraction are the energy required to flow the streams across the membrane, the cost of the solvent, and the energy cost for regenerating the solvent (with methods such as evaporation). While this method has been shown to be more cost effective than air-

stripping and adsorption using activated carbon [86], it requires the use of hazardous solvents, and – like adsorption – merely transfers the contaminant to another phase without degrading it. Furthermore, the often dilute concentrations of COCs in soils and groundwaters require high solvent flow rates for efficient extraction, which drives up energy costs [86], [87].

To subvert the challenges facing the removal of azo dyes and COCs with conventional membrane separation, membrane technologies using mechanisms other than size exclusion such as adsorption, biodegradation, membrane distillation, and degradation by reactive oxygen species (ROS) have been explored [89]–[92].

2.4 Electrically Conductive Membranes

2.4.1 Introduction to Conductive Membranes and Their Benefits

Recent work has shown that applying an electric field across a membrane can combat organic and colloidal fouling. Additionally, the application of small pulsed electric potentials to a surface has been shown to prevent the attachment of bacteria, and thus prevent the onset of biofouling [14], [40]–[43]. This phenomenon is not yet completely understood, as several mechanisms likely contribute to its result. For instance, the application of negative (cathodic) potentials has been shown to repel negatively charged bacteria through electrostatic interactions [39], [93], [94]. Alternatively, the application of negative potentials to electrodes in an aqueous medium can generate ROS [51], [95] capable of killing bacteria that would otherwise foul the surface [51], [96]. Whatever the mechanism, the success of this phenomenon in fouling mitigation has led to the investigation of electrically conductive membrane materials.

Aside from biofouling prevention, electrically conductive membranes have been investigated for their effectiveness in applications as electrodes, for charged particle selectivity,

for generating ROS in solution, and in a variety of other electrocatalytic separations [39], [51], [52], [94], [97], [98].

2.4.2 Graphitic Materials for Conductive Thin Film Surface Composites

While modern conventional membranes are commonly made from polymers, conducting polymers such as polypyrrole are limited in their use as a membrane material by physical properties that result in poor processing and separation characteristics [39]. Membrane thin film surface composites made of conductive materials such as graphene oxide (GO) and carbon nanotubes (CNTs) have received interest as an alternative to conductive polymers and their limitations [44], [39], [45]. CNTs are essentially 2D graphene seamlessly rolled into a 3D tube configuration with one or multiple walls. These materials owe their high conductivity to the delocalized nature of their pi electrons, and their high length-to-diameter aspect ratios (typically >1000:1) [39], [93], [94], [97], [99]. Dispersions of CNTs can be easily vacuum filtered onto the surface of a polymeric support membrane to form a porous, electrically conductive thin films capable of simultaneously preventing biofouling, and removing azo dyes through electrochemical filtration, adsorption, and the production of ROS in solution [39], [97].

2.5 Growing Reactive Nanoparticles

2.5.1 Zero Valent Iron

Both chlorinated organics and azo dyes can be degraded through redox reactions with strong reducing agents. Among these reducing agents, elemental iron in its zero valent state (Fe^0 or ZVI) remains an established choice for applications in remediating groundwaters and soils contaminated by chlorinated organics, as well as textile effluents contaminated by azo dyes [22], [24]–[27][28]. ZVI stands out from other reducing agent remediation technologies due to iron's

natural abundance, low cost, high reducing potential (E^0= -0.44 V), low toxicity, and capacity to adsorb compounds such as dyes and heavy metals [21], [27], [30]–[32].

2.5.2 Reactive Nano Zero-Valent Iron Particles

The efficacy of ZVI and other reactive metals can be further improved by synthesizing those materials into spherical particles with diameters in the nanoscale. Nano zero-valent iron (nZVI) has been the focus of more recent work due to its increased reactivity [22], [26], [29], [33]–[35]. nZVI and other nanoparticles are relatively more reactive than their macroscale counterparts because of their increased surface area to volume ratios. This is because as particle size decreases, there is an increase in the proportion of atoms on the surface of that particle available for reaction, adsorption, etc. [36].

The high reactivity presented by nanoscale particles has been explored for a variety of materials and applications. For instance, silver nanoparticles have proven to be effective in antimicrobial sterilization [25], [36], [100], [101], and have been investigated alongside gold and platinum nanoparticles for applications in catalysis [49]. Titanium dioxide nanoparticles have also been applied as adsorbents [49], as well as used for coatings that impart UV protection and self cleaning properties [36].

nZVI particles generally have diameters less than 100 nm and exhibit a core-shell structure. While the nanoparticle core consists of highly reactive zero-valent iron, there exists an outer shell of Fe^{2+} and Fe^{3+} oxides and hydroxides [24], [26], [102].

2.5.3 Methods for nZVI Synthesis

The synthesis of nZVI particles can generally be categorized into top down or bottom up approaches. Top down methods involve physical and chemical methods of breaking down – and

in some cases chemically reducing – iron to a nanoscale zero-valent state. The simplest top down method consists of mechanically grinding (or milling) macroscale bulk ZVI down into the nanoscale [102][103]. Thermal reduction is a technique in which iron oxide nanoparticles are reduced to nZVI at high temperatures (> 500℃) by gases such as H_2, CO_2, and CO that are produced from the thermal decomposition of carbon based materials [36][104].

Bottom up methods facilitate the growth of nZVI particles from iron salts. The most common bottom up methods use strong reducing agents such as sodium borohydride to precipitate nanoparticles from iron ions in solution [32], [105]. This method is highly effective, however, the toxicity and cost of sodium borohydride has encouraged researchers to explore polyphenolic plant extracts as an environmentally friendly reducing agent alternative [36], [55]. Thermal reduction can also be applied as a bottom up method, by instead using hydrous iron salts as the source for the precipitated nanoparticles [36]. Electrolysis is a third bottom up method that produces nZVI from iron salts in solution using an electrochemical cell. Positively charged iron ions are reduced into nZVI particles at the cathode, and subsequently removed with ultrasonication [80]. Electrolysis is relatively fast and cost effective when compared to chemical reduction, but often results in nanoparticle aggregation during formation at the cathode [106].

2.5.4 Challenges Surrounding Nanoparticle Technologies

nZVI nanoparticles rapidly homo-aggregate due to their strong magnetic properties and low surface charge [32], [38], [102], [107]. Aggregation reduces their high surface area to volume ratio, which causes a significant loss in reactivity [26], [31], [32], [34], [37], [38]. Furthermore, colloids formed from nZVI aggregates have significantly reduced mobility in soils, which limits their use for applications such as in the in-situ remediation of groundwaters [26], [102].

A second limiting factor that nZVI faces is passivation, which is the inevitable loss of the nanoparticle's reactivity caused by donating electrons to other species [22]. nZVI particles are thus a one-time-use nanomaterial, requiring continuous resupplying to treat large volumes of contaminated water.

2.6 Stabilizing Reactive Nanoparticles

nZVI can be stabilized against aggregation through the application of surface coatings, doping the nanoparticles with other metals, and immobilizing the particles on supports.

2.6.1 Surface coatings

A wide variety of compounds have been tested as nanoparticle coatings to encourage their dispersion and consequently prevent aggregation [102]. Materials chosen for coatings are generally those that suppress the tendency and/or ability of the nanoparticles to agglomerate by electrostatic, magnetic dipole-dipole, and DLVO interactions [107], [108]. Surface coating molecules achieve this stability by enhancing the repulsive forces between particles with either or both of electrostatic and steric stabilization. In electrostatic stabilization, charged molecules are adsorbed to the metal nanoparticle surface to create a double layer that repels the other stabilizer-covered particles. Steric stabilization, on the other hand, relies on coatings with external structures that physically impede particle attraction, as well as by osmotic force [32], [37], [108].

Stabilizers can be added during the nano-particle growth before aggregates are formed (pre-agglomeration) or after nanoparticles have grown and aggregated (post agglomeration) [32]. In both cases the addition of a stabilizer can result in nanoparticle dispersion, however, pre-agglomeration addition has been shown to be more successful in doing so [104]. Table 2.1 below

provides an overview of several different types and examples of surface coatings used to stabilize nZVI [7], [28], [116]–[123], [108]–[115].

Table 2.1. nZVI surface coating types with examples [7], [28], [112]–[119], [104]–[111].

Coating Type	Examples
Hydrophilic biopolymers	Starch, guar gum, alginate, aspartame, chitosan
Natural Organic Matter (NOM)	Humic acid
Polyelectrolytes	Carboxymethyl cellulose (CMC), polyacrylic acid, resins, block coplymers
Oil-based Microemulsions	Food grade surfactant

Coatings are of further use for lessening the passivation of nZVI that would occur through side reactions. nZVI coated with polyelectrolytes such as CMC, are less prone to side reactions with dissolved oxygen and oxygen rich compounds in solution, and therefore allow the nanoparticles to save their reactivity for the target compounds [32], [36], [102], [109]. Naturally, surface coatings detract slightly from nanoparticle reactivity by covering a portion of their available surface area, however, the reactivity of stabilized particles that remain dispersed exceeds those that are uncovered but have been allowed to aggregate [32].

2.6.2 Substrate-Supports

With the proper substrate, nanoparticles can be stabilized against aggregation through steric and electrostatic mechanisms [48]–[50]. Suitable substrates for nZVI and other metal nanoparticles are those that have a high surface area and negatively charged functional groups to

attract the positively charged metal ions and serve as nucleation sites during nanoparticle growth [31], [35], [37], [49], [50], [124], [125]. Nano-porous materials can provide stabilization through the physical segregation of nZVI particles in their structure [49]. A variety of solids have been explored as substrates for stabilizing nanoparticles , such as cellulose nanocrystals and nanofibers [49], [50], [126], silica [122], [127], [128], high surface area pyrolyzed carbon materials such as biochar and activated carbon [129], [130], and graphite materials such as graphene, and carbon nanotubes [31], [46], [47].

2.7 Objectives

The aim of this project was to fabricate a porous, electrically conductive, catalytic, reactive surface composite for removing an azo dye model contaminant in solution. The nZVI particles were grown using a bottom up chemical reduction method and stabilized by a network of COOH-functionalized carbon nanotubes serving as a substrate. The specific goals of this research include:

- Proof of concept validation for using an applied voltage to regenerate embedded nZVI reactivity for the enhanced electrocatalytic degradation of contaminants in a simple batch system.
- Demonstrating the ability of nZVI-CNT surface composite membranes to electrochemically degrade azo dyes in solution under an applied voltage in batch and continuous systems.
- Modelling the contaminant removal performance of nZVI-CNT surface composite membranes in a batch system, to analyze and optimize the contributions of operating parameters such as applied voltage and nZVI content.

Chapter 3

Proof of Concept Validation of the Electrocatalytic Properties of nZVI-CNT Surface Composites through Dye Removal in a Batch System

Abstract

Azo dyes and Chlorinated Organic Compounds (COCs) like trichloroethylene (TCE) are environmental contaminants found in textile industry effluents and groundwater sites respectively. Both compounds are carcinogenic to humans and hazardous to the environments they contaminate and are difficult to treat by conventional wastewater processes. In this study, electrocatalytically active nanocomposite membranes were fabricated and evaluated for their ability to remove azo dyes. Nano zero-valent iron (nZVI) particles were grown and stabilized within a network of dispersed single and double-walled carbon nanotubes (CNTs), and this mixture was filtered onto the surface of a microfiltration PES support membrane to form a porous, conductive, reactive surface nanocomposite. These catalytic surface nanocomposites were tested as a cathode alongside a graphite anode for their ability to remove methyl orange (MO) dye in a batch system under -2 V applied voltage. In a well-mixed batch, it was found that complete removal of 0.25 mM MO (7.5 mMoles in 30 mL) by the charged membranes occurred within 2-3 hours of operation. The performance of these nZVI-CNT cathodes alongside controls suggests that the application of an applied current regenerates the spent reactivity of the embedded iron nanoparticles. Continuous regeneration of nZVI reactivity on a membrane surface offers substantial advantages over single-use approaches for the treatment of azo dyes and COCs in solution.

3.1 Introduction

Chemical reductants such as ZVI have been proved to be effective in remediating organics such as azo dyes and COCs into less toxic compounds by degrading their characteristic bonds (their azo linkages and chloride bonds respectively) [23], [29], [59]. Among these technologies, nZVI has emerged as an increasingly attractive option for facilitating reductive remediation of these organics, due to its enhanced reactivity [26], [35], cheap source material, and non-toxicity [4], [76]. A mechanism for the direct and ROS mediated reduction of azo dyes and COCs using zero valent iron is shown in Figure 3.1.

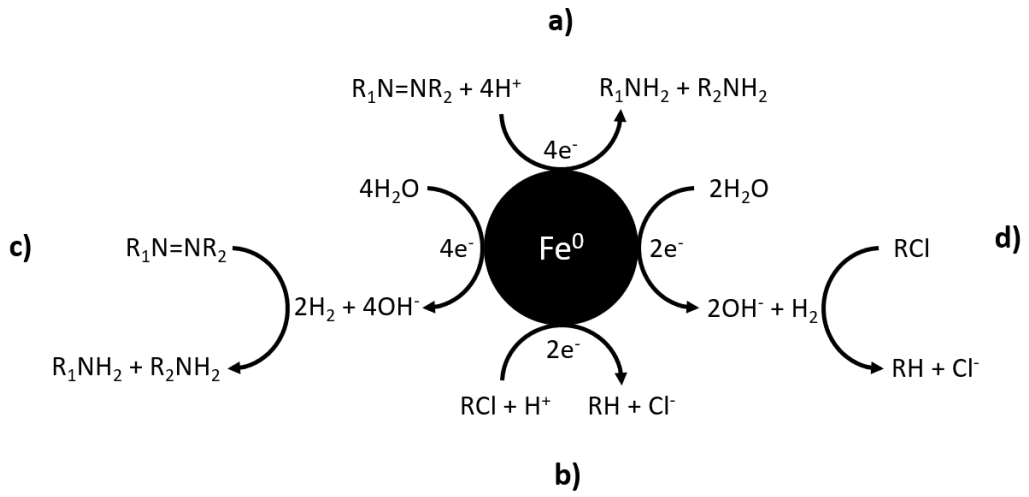

Figure 3.1. Mechanisms for the degradation of azo dyes by a) direct reduction and c) ROS mediated reduction, and mechanisms for the degradation of COCs by b) direct reduction and d) ROS mediated reduction.

Unfortunately, the nZVI's ability to remediate contaminants is limited by two main problems. The first of these problems is the tendency of nanoparticles to homo-aggregate into colloids, resulting in the loss of high surface area to volume ratio and thus decreased reactivity [32], [131]. Secondly, nZVI's high potential for oxidation allows many oxygen rich compounds in solution can scavenge its reactivity, limiting its potential for reducing and remediating target contaminants [22], [36], [38]. Furthermore, even if nZVI were able to selectively reduce contaminant compounds in solution, it still faces the issue of loss in reactivity through reducing contaminants in its intended operation [22]. Thus, technologies utilizing nZVI lack the ability to operate continuously without nanoparticle replacement.

Recent work has shown that nanoparticle aggregation can be mitigated by growing and stabilizing those particles on surfaces and in the pores of substrates [31], [35], [37], [49], [50], [124], [125]. CNTs have been investigated as a nanoparticle stabilizing substrate [132] due to their high surface area, and ability to possess functional groups that aid in stabilization [79], [84], [132].

This study focuses on developing conductive CNT membrane surface composites with embedded stabilized catalytic nZVI particles for remediating methyl orange in solution. The permeable network of CNTs in this surface composite layer allows for the passage of a contaminated feed, while the nZVI particles stabilized in the CNT network facilitate a reduction reaction to degrade the contaminants. Furthermore, when a negative voltage is applied to the conductive surface composite, the CNTs function as an electrode capable of both directly reducing azo dyes in solution and channeling electrons to regenerate the reactivity of the embedded nZVI particles. Thus, with an applied pressure and voltage, nZVI-CNT membranes can continuously electro-catalytically degrade azo dyes from a aqueous feed stream.

3.2 Materials and Methods

3.2.1 Materials

All solutions used for synthesis, characterization, and testing were prepared in de-ionized water from a Sartorious Arium Mini device. Single/double walled COOH-functionalized carbon nanotubes (1-4 nm diameter, 5-30 μm length, 2.73 wt% functional content) were purchased from Cheaptubes. The following chemicals used were all of lab grade purity (> 98% pure). Iron sulfate pentahydrate and sodium chloride were both purchased from Sigma Aldrich. Sodium borohydride was purchased from Alfa Aesar.

All nitrogen gas used came from Air Liquide compressed nitrogen tanks (100% pure). The circular flat sheet polyether sulfone microfiltration membranes were purchased from Sterlitech (0.45 μm pore size, 47 mm diameter). Methyl orange powder was purchased from Sigma Aldrich.

3.2.2 Catalytic Membrane Composite Preparation

Single/double walled COOH-functionalized carbon nanotubes were dispersed in a round bottom flask of deoxygenated (DO) water using a QSonica probe sonicator for 30 minutes effective time (two seconds dormant alternating with two seconds active). During sonication, nitrogen gas was bubbled into the flask at low pressure to maintain a nitrogen-rich solution and minimize the concentration of dissolved oxygen.

After sonication, the flask was closed with a septum cap. Nitrogen was continuously bubbled into the solution through a needle which pierced the septum and extended into the solution. A second shorter needle which pierced the septum did not reach the solution and was used as a pressure release. Low pressures and low gas flow rates were used to facilitate bubbling/stirring and to maintain a nitrogen atmosphere within the flask to prevent the oxidation of nZVI in

subsequent steps. Iron Sulfate Pentahydrate was added in a ratio of 3:1 Fe^{2+} ions to -COOH functional groups of the dispersed CNTs. After an hour of mixing time – over which the positively charged iron ions became associated with the negatively charged functional groups – sodium borohydride dissolved in DO water was added dropwise to the round bottom flask at a controlled rate of 0.5 mL/minute for 10 minutes using a KdScientific syringe pump. An appropriate amount of $NaBH_4$ was added to achieve a BH_4^-: Fe^{2+} ratio of 2:1, with 10% excess of $NaBH_4$ to account for undesirable side reactions with water. The $NaBH_4$ reduces iron ions into zero-valent iron nanoparticles on the surface of the CNTs. The mixture was kept bubbling under nitrogen for one hour past the addition of sodium borohydride to ensure the reaction reached completion. Once the reaction was assumed complete, the round bottom flask containing the dispersed nZVI-CNT mixture was sealed under nitrogen atmosphere.

In an N_2-enriched glovebox, the nZVI-CNT mixture was filter-deposited onto the surface of 0.45 μm pore size flat sheet polyether sulfone (PES) membranes using a vacuum pump following the same protocol as previously published [133]. The surface composites of each membrane consisted of 10 mg of nZVI-CNT mixture, and were each approximately 35.5 mm in diameter. The newly fabricated nZVI-CNT membranes were dried under the ambient N_2 environment inside the glovebox then stored separately in air. It should be noted that during storage, the nZVI within the membrane surface composite oxidized due to exposure to ambient air. Exposure to air was expected to cause the formation of a shell of iron oxides and hydroxides around an inner core of nZVI that will slowly oxidize over time.

3.2.3 Membrane Characterization

The prepared catalytic membranes and the nZVI-CNT material used to fabricate them were characterized with both Scanning Electron Microscopy (SEM) and Transmission Electron

Microscopy (TEM). For TEM studies, newly prepared nZVI-CNT mixtures were diluted with DO water before being drop-deposited and dried on the surface of holey carbon-coated copper grids inside a glovebox under a nitrogen atmosphere. These grids were subsequently analyzed under TEM-EDS (Jeol2010F) to show the structure and elemental composition of the catalytic composite material. For examining the catalytic membrane cross-section, nZVI-CNT membranes were cut into small pieces (< 20 mm^2) and frozen with liquid nitrogen for approximately 5 minutes under vacuum. These frozen membrane pieces were cracked in half using tweezers, sputter coated with 5 nm thick coatings of Au and imaged under SEM (JEOL JSM-7000F).

Sheet resistivity measurements were taken using a HALL HL5500PC four point-probe device to measure the electrical conductivity of the nZVI-CNT membrane surface composites. These sheet resistivities were converted to conductivity values by taking the inverse of each measurement and dividing by an average surface composite thickness estimated from cross-sectional SEM images.

Catalytic membrane iron content was determined through a mass balance and measurements taken using Inductively Coupled Plasma Optical Emission Spectrometry (ICP-OES). These tests analyzed the permeate samples obtained from the vacuum filtration step of the catalytic surface composite synthesis process. The permeates were diluted to volumes of 12 mL and tested with a Vista-Pro CCD Simultaneous ICP-OES device over a measuring range of 20 – 100 ppm. Once the iron concentration of the permeate is known, the mass of iron in the surface nanocomposite can be calculated by subtracting the mass of iron in the permeate sample from the iron assumed to be in the aliquot of well mixed nZVI-CNT mixture filter deposited onto the PES support membrane.

3.2.4 Electrochemical Batch Removal of Methyl Orange Dye

The azo dye, methyl orange (MO), was chosen as a model contaminant. The UV-Vis absorbance of MO is approximately linearly proportional to its concentration. A calibration curve (Figure S1) was generated using a UV-Vis spectrophotometer to determine the concentration of MO after exposure to the catalytic membranes. Figure 3.2 shows the experimental batch system, in which a conductive membrane composite (nZVI-CNT or CNT) as the working electrode, and graphite strip (VWR, $l \times w \times t$ = 5 cm × 2 cm × 0.5 mm) as the counter electrode electrochemically degrade a batch of MO. The electrodes were spaced 3 mm apart with a parallel overlapping area of ~3.8 cm^2.

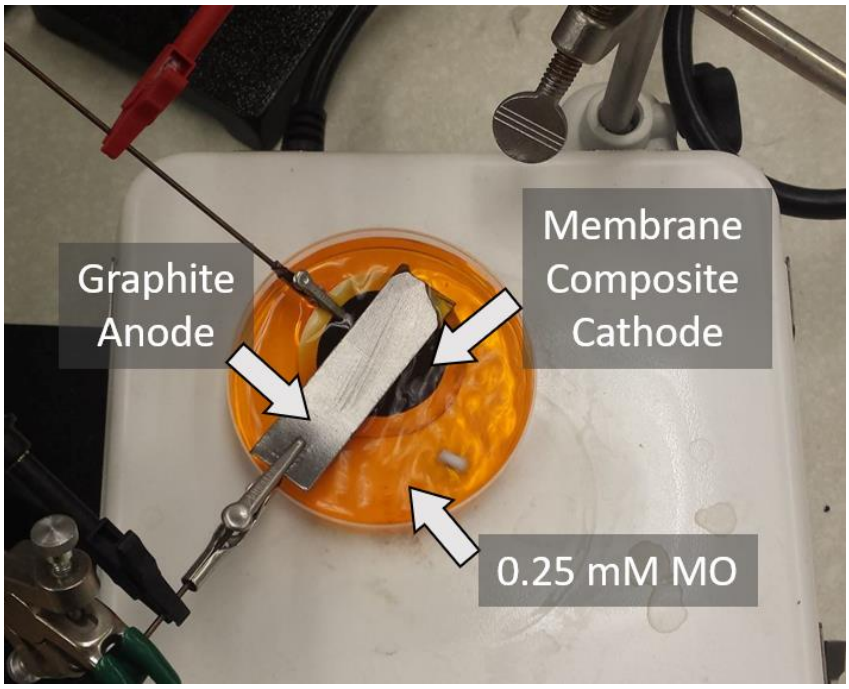

Figure 3.2. The experimental setup for testing nZVI-CNTs performance in removing MO in solution under an applied voltage.

A constant negative voltage (-2 V) was applied between the membrane composite cathode and the graphite strip anode using an Autolab potentiostat/galvanostat to form an electrochemical cell. Over the course of a three-hour period, 200 µL samples were taken from the well-mixed batch (stirring at 900 rpm) at 10-minute intervals. The absorbances for these samples were measured at 464 nm in a Tecan Spark 10M UV-Vis Spectrophotometer, and the corresponding concentration was calculated from the absorbance-concentration calibration curve (Figure S1).

3.2.5 Cyclic Voltammetry

Cyclic voltammetry (CV) tests were conducted to assess the nature of the electrochemical reactions taking place in the batch and continuous MO removal systems. Using an experimental setup identical to the batch removal system, a CV test was conducted between -2 V and 2 V at a scan rate of 10 mV/s using an Autolab Potentiostat. A sufficient amount of sodium chloride was dissolved in the batch system to ensure a solution conductivity of 1000 μS/m.

3.3 Results and Discussion

3.3.1 nZVI-CNT Membrane Composite Morphology

Dark-field TEM images show CNTs with adsorbed nZVI particles (Figure 3.3), which are accompanied by TEM-EDS scans showing the carbon and iron content. The elemental analysis of this image yields carbon, oxygen, and iron atomic percentages of 56.3%, 13.7%, and 5.5% (with the remaining percentage being composed of copper from the TEM grid, and Na from the addition of $NaBH_4$ during nanoparticle synthesis). Figure 3.3 and its corresponding atomic % breakdown

confirm that the structure observed on the CNTs is an iron nanoparticle with a diameter of ~57 nm.

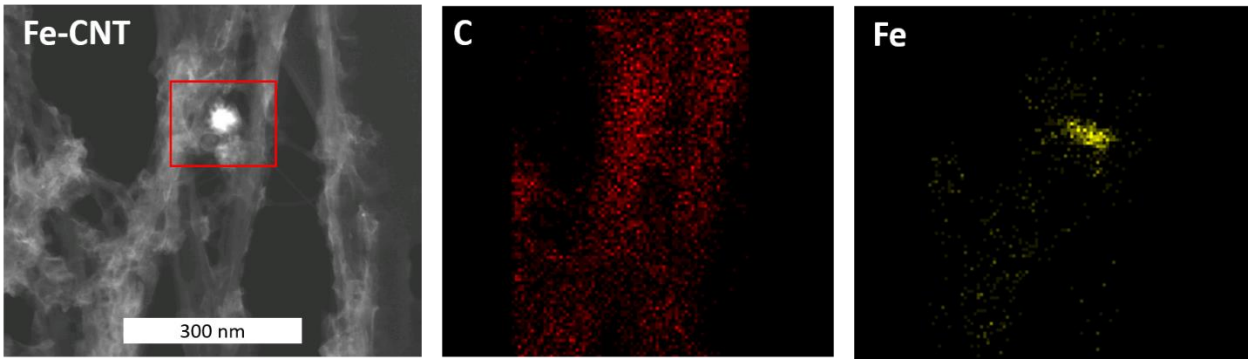

Figure 3.3. TEM-EDS images showing an nZVI-CNT mixture (left) and its main elemental composition in terms of carbon (middle) and iron (right).

3.3.2 Catalytic Membrane Conductivity and Iron Content

The results of the conductivity tests performed are shown in Figure 3.4 (left), which show that membranes with nZVI-CNT and CNT composites are highly conductive (40 098 $\pm$ 3570 S/m, and 97 877 $\pm$ 7714 S/m respectively.

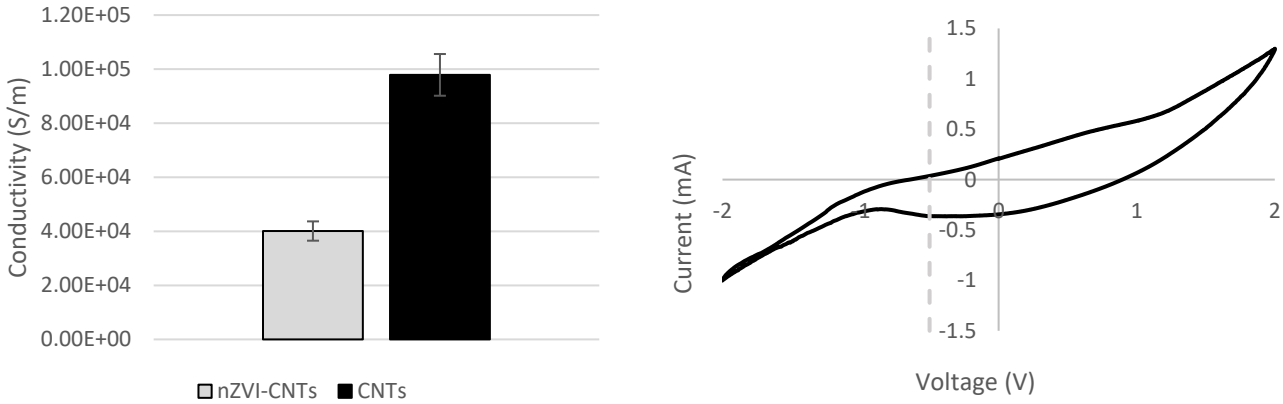

Figure 3.4. Left: Conductivity results from 4-point probe measurements on nZVI-CNT and CNT membrane composites, and right: Cyclic voltammetry on the batch removal system using an nZVI-CNT cathode, with a grey dotted line shown to outline the MO reduction peak.

These results in Figure 3.4 (left) indicate that the 10 mg nZVI-CNT membrane composites are on average 2.4-times less conductive than 10 mg CNT membrane composites. We hypothesize that the lower nZVI-CNT composite conductivity values are a result of the presence of oxidized iron within the composite. Although nZVI nanoparticles are highly conductive, the corrosion layer of iron oxides and hydroxides that develops on the surface of these nanoparticles with exposure to oxygen in storage is electrically insulating. Incorporating an electrically insulting material to the surface composite reduces the overall conductivity of the network. While nZVI-CNT membrane composites are less conductive than those made up solely of CNTs, the catalytic membrane thin films are still highly conductive and effective as an electrode material for facilitating the electrochemical degradation of azo dyes and COCs [51]. Figure 3.4 (right) shows the results of a CV scan between -2 V and 2 V using an nZVI-CNT cathode, a graphite strip anode, and a 1 mM MO solution brought to 1000 μS/m through the addition of NaCl. The peak around -0.5V in the scan is indicative of the direct reduction of methyl orange occurring at the cathode [64].

The mass of iron remaining in the surface composite was determined by measuring the iron concentration in the liquid permeates of the vacuum deposition stage during the membrane surface composite fabrication process. ICP-OES was used to quantify the permeate iron content. The results of these measurements yielded negligible concentration of iron in the permeate samples. We concluded that the iron vacuum deposited onto the membrane surface remains either within the CNT network of the surface composite, or within the pores of the PES support membrane.

3.3.3 MO Batch Removal Performance of Catalytic Membranes

Membranes with catalytic nZVI-CNT surface composites were first tested in a batch system rather than a continuous system for a few important reasons. First and foremost, a batch system, lacks parameters that complicate comparisons of experimental results, such as feed pressure and flow rate. Since the retention time of MO in a continuous membrane flow cell affects the extent to which the model contaminant is degraded, differing flow rates between the various experiments complicates comparisons between them. Thus, the relatively simpler batch system is preferable for examining the ability of an applied voltage to regenerate the reactivity of the embedded nZVI particles. Secondly, a batch system allows for the examination of a given membrane composite's affinity to adsorb MO over time, and further distinguishes the contributions of adsorption and chemical reaction.

Figure 3.5 shows the concentration of 0.25 mM MO over a three-hour batch test using conductive membrane composites as a cathode and a graphite strip as an anode. 0.25 mM (~82 ppm on a mass basis) was chosen to reflect common textile industry effluent concentrations (50 – 80 ppm) [134]. This data corresponds to triplicate tests for batch removal using an nZVI-CNT surface composite membrane as well as data for three controls: membranes without nZVI, without applied voltage, and without nZVI or applied voltage. The systems, shown in Figure 3.5 were tested in triplicate, with each test using a new membrane sample.

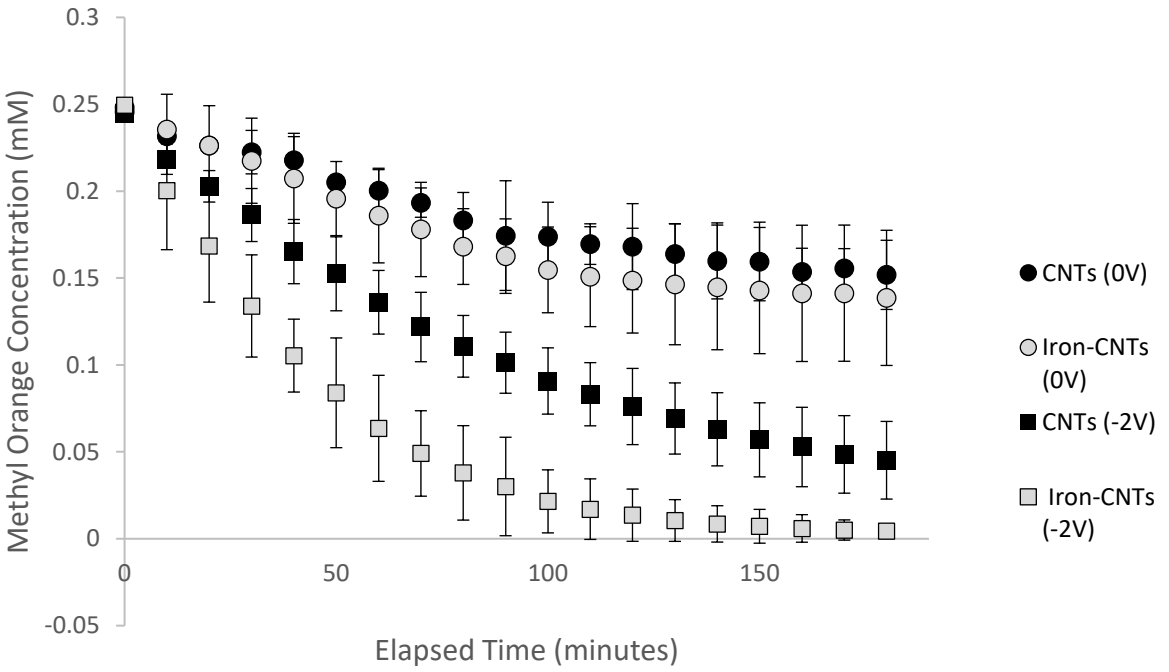

Figure 3.5. Results for batch removal of MO using nZVI-CNT cathodes (grey) and CNT cathodes (black), operating at -2V (squares) or with no applied voltage (circles). Error bars represent the 95% confidence interval.

From the nZVI-CNT (-2 V) test results displayed in Figure 3.5, MO dye concentration C over time t can be described as decaying exponentially from the initial concentration C_0 by the relation: $C = C_0 e^{\alpha t}$, where α is some parameter $\alpha < 0$ encapsulating the contributions of regenerated and/or added catalytic nZVI reactivity, direct reduction at surface of the CNTs (in the presence of an applied voltage), ROS reactivity, and adsorption. A model describing the decrease in MO concentration over time in the presence of an nZVI-CNT cathode and -2 V applied voltage was fit with linear-in-parameters regression and is given by $C = 0.25e^{-0.023t}$ ($R^2 = 0.996$).

Comparing the series in Figure 3.5, it is evident that MO removal is achieved in all systems with and without nZVI and with and without applied voltage. However, the rate of MO removal

varies significantly. Applied voltage and the presence of nZVI both contributed to greater MO removal. With no applied voltage, both systems with and without iron-particles managed to remove MO, however, the systems with nZVI achieved higher removal than those without. This indicates that the presence of nZVI enhances MO removal. The removal of MO without applied voltage can be explained by two phenomena. Firstly CNTs and iron nanoparticles (in both nZVI and iron oxide states) have demonstrated high affinity for the adsorption of dyes [29], [35], [52]. Secondly, MO removal in the absence of applied voltage could indicate the reduction of MO by nZVI remaining beneath the oxidized shell covering the nanoparticles [26]. The added adsorptive capacity and remaining reactivity of nZVI particles could provide evidence as to why systems with nZVI-CNT cathodes remove more MO than systems with CNT cathodes. However, it should be noted that at the 95% confidence level, there is currently insufficient statistical evidence to suggest that a difference exists in the true mean removal of MO from systems using nZVI-CNT composites and systems using CNT composites when there is no applied voltage to the system.

The results of Figure 3.5 indicate that applying -2 V to the batch system causes a large increase in MO removal and highlights the impact of CNT membranes with nZVI as compared with those without. Comparing the two systems without nZVI – labelled CNTs (0 V) and CNTs (-2 V) on Figure 3.5 – it is evident that CNT systems with an applied voltage achieved increased MO removal. This elevated MO removal is due to the reductive electrochemical degradation of the dye at the surface of the CNT cathode [64]. Furthermore, examining the nZVI-CNT results with -2 V applied, elevated removal of MO is observed when nZVI is included and a voltage is applied, suggesting that a synergistic effect exists between the two. This finding lends support to the hypothesis that an applied voltage regenerated the reactivity of the nZVI particles thereby causing enhanced electro-catalytic MO removal. Furthermore, the aforementioned exponential

rate at which the nZVI-CNT system removes MO dye resembles the kinetics of nZVI's degradation of azo dyes in the literature [29]. This elevated removal allows an nZVI-CNT system with -2 V applied to fully remove 0.25 mM MO from a 30 mL batch within 2-3 hours (100% removal), while a CNT system with -2 V applied only reduces MO concentrations of batches with identical specifications to 0.05-0.07 mM within 2-3 hours (70-79% removal).

3.4 Conclusions

nZVI nanoparticles can be grown and stabilized onto a network of functionalized carbon nanotubes. This nZVI-CNT mixture can be readily deposited onto a support membrane to form a conductive, continuously reactive, and adsorptive thin film composite. Results of batch tests using conductive membrane surface composites as a cathode and graphite foil as an anode have shown that these membranes can remove MO by electrochemical reaction and adsorption, at an exponentially decaying rate. These same results indicate that an applied voltage to a membrane surface composite possessing nZVI enables increased removal of MO. The enhanced removal of MO through an applied voltage to embedded nZVI nanoparticles suggests the partial restoration of nZVI reactivity lost to passivation. With -2 V applied to a system using a 10 mg nZVI-CNT cathode, batches of 0.25 mM MO can be fully removed within 2-3 hours.

Chapter 4

Application of Catalytic Membranes in a Continuous Dead-End Flow System

Abstract

Effluents from textile industry processes using azo dyes require continuous treatment to comply with increasingly strict environmental regulations. In this study, membranes with conductive catalytic nZVI-CNT composites are employed as electrochemically reactive barriers to continuously remediate a pressurized feed of methyl orange dye. These tests were conducted in a custom-built dead-end flow cell at feed pressures ranging between 20 and 80 psi, with a -2 V voltage applied to the electrochemical cell formed by a membrane surface composite cathode opposite a graphite strip anode. Systems using nZVI-CNT membranes achieved ~87 mole % removal of methyl orange and demonstrated a 2.7 times greater removal rate than batch tests of analogous parameters, and 1.6 times greater than other continuous tests using membrane surface composites that lacked nZVI. Furthermore, the application of voltage to the membrane thin film surface composite increases the transmembrane flux through system, allowing for increased throughput at a given feed pressure. The results of these experiments show promise in the continuous removal of contaminants from wastewaters through reductive degradation, such as azo dyes and chlorinated organic compounds.

4.1 Introduction

Membrane separations have become prevalent and ubiquitous in modern wastewater treatment applications. RO membranes have proven to be capable of removing dyes and chlorinated solvents from wastewaters [15]–[18]. However, this conventional method of membrane separation is plagued by issues such as high transmembrane pressure gradients (and thus high energy costs), membrane damage due to concentration polarization, and biofouling [14], [16]–[18], [71], [73], [77].

Electrically conductive membranes have shown promise in preventing biofouling [14], [40]–[43]. Such membranes have been prepared by filter depositing graphitic materials such as CNTs into conductive, porous thin films on the surface of conventional polymer support membranes. Additionally, CNT films have been shown to facilitate the electrochemical degradation of dyes under an applied voltage.

Nano zero-valent iron particles represent an alternative technology for remediating COCs and azo dyes and can be grown and stabilized on the carboxylic acid groups of functionalized CNTs. Furthermore, the results of studies presented in Chapter 3 suggest that the reactivity of nZVI embedded within a thin film nanocomposite of CNTs can be regenerated through the application of a negative voltage. These regenerated nanoparticles add electro-catalytic reactivity to the electrochemical capabilities of the CNTs for enhanced removal of organic contaminants under an applied voltage.

The objective of this work was to develop a conductive, porous, reactive nanoparticle-embedded membrane surface composite capable of remediating an azo dye feed solution. The membrane surface composite achieves this remediation using electrochemical reaction under an

applied voltage rather than conventional size exclusion. The performance of these membranes regarding membrane flux, permeability, and contaminant removal was tested in a continuous dead-end flow configuration under an applied voltage. The reliance of contaminant removal on an applied voltage for electrochemical degradation rather than size exclusion presents the opportunity for operations using membranes with larger pores. This effectively means that the application of a low negative voltage undercuts the need for vastly greater transmembrane pressures, and thus offers savings in terms of operating energy requirements.

4.2 Materials and Methods

4.2.1 Materials

Pure water flux measurements were conducted with reverse osmosis (RO) filtered water. Apart from these pure water flux tests, all solutions used for synthesis, characterization, and testing were prepared in de-ionized water from a Sartorious Arium Mini device. Single/double walled COOH-functionalized carbon nanotubes (1-4 nm diameter, 5-30 μm length, 2.73 wt% functional content) were purchased from Cheaptubes. The following chemicals used were all of lab grade purity (> 98% pure). Iron sulfate pentahydrate and sodium chloride were both purchased from Sigma Aldrich. Sodium borohydride was purchased from Alfa Aesar. Sodium dodecyl sulfate was purchased from Anachemia.

All nitrogen gas used came from Air Liquide compressed nitrogen tanks (100% pure). The circular flat sheet polyether sulfone microfiltration membranes were purchased from Sterlitech (0.45 μm pore size, 47 mm diameter). Methyl orange powder was purchased from Sigma Aldrich.

4.2.2 Catalytic Membrane Composite Preparation

The procedure to fabricate nZVI-CNT membrane surface composites for continuous tests was nearly identical to that for the batch tests explained in Section 3.2.2, with three notable differences. Firstly, the line of nitrogen gas placed into the solution for mixing and preserving a deoxygenated environment in the process for fabricating membranes for batch tests was instead kept above the solution in the void space of the round bottom flask. Mixing was instead accomplished by bath sonication. Secondly, membrane composites used for continuous tests contained 4 mg of nZVI-CNT, rather than 10 mg. A lower composite mass was chosen for the continuous tests to achieve higher fluxes, to increase membrane fabrication throughput, and to lower the extent to which contaminant removal was facilitated by adsorption rather than electrochemical reaction. Thirdly, sodium dodecyl sulfate (SDS) was added in a 1:1 mass ratio with CNTs before the probe sonication step to ensure proper dispersion of the CNT network. While the addition of SDS was assumed to decrease surface composite conductivity, it is necessary for maintaining nZVI-CNT dispersion to fabricate uniform membrane surface composites with reproducible permeabilities.

4.2.3 Membrane Characterization

The prepared catalytic membranes and the nZVI-CNT material used to fabricate them were characterized with Scanning Electron Microscopy (SEM). To examine the catalytic membrane cross-section, nZVI-CNT membranes were cut into small pieces (< 20 mm^2) and frozen with liquid nitrogen for approximately 5 minutes under vacuum. These frozen membrane pieces were cracked in half using tweezers, sputter coated with 5 nm thick coatings of Au and imaged under SEM (JEOL JSM-7000F).

4.2.4 Membrane Flow Characterization

The permeabilities of the membranes possessing catalytic surface composites were determined from pure water flux measurements. In these experiments a membrane was placed inside a Sterlitech flow cell (37 mm inner diameter) and subjected to a pressurized flow of DIW from a reservoir. The pressure gradient driving this flow was supplied by pressurized nitrogen gas. Before testing, each membrane was pressurized for one hour under 90 psi. Flux was measured for each pressure in the range of 20 – 80 psi at 10 psi increments. When testing at a given pressure, the cumulative mass of permeate was recorded at 10 second intervals up to one minute. From these measurements, the average volumetric flux in each interval was calculated. Flux was calculated using the surface area of the membrane. Membrane permeability was determined from the linear regression of the slope of the flux measurements plotted against their corresponding pressures.

4.2.5 Continuous Electrochemical Removal of Methyl Orange Dye

Figure 3.1 (a) and (b) show the electrochemical membrane flow cell and its schematic representation, respectively. Within the custom-built dead-end electrochemical flow cell, the electro-catalytically active membrane is positioned at the bottom of the cell chamber opposite a graphite anode. A more detailed description of the electrochemical flow cell can be found in the SI and is similar in design to several other cells in the literature [94], [135], [136].

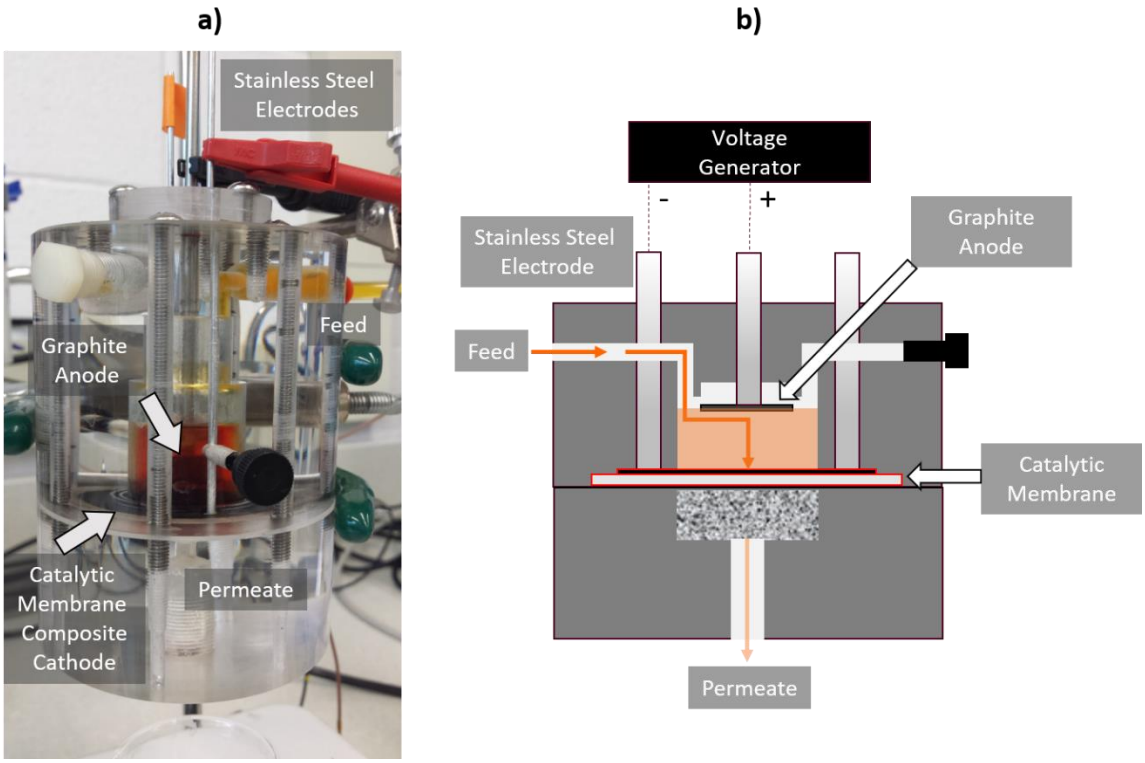

Figure 4.1. a) A visual and b) a schematic of the continuous dead-end flow system used to test the catalytic membrane's performance in electrochemically degrading MO.

The membrane separated a N_2-pressurized MO feed from an external reservoir. The spacing between cathode and anode can be adjusted as the graphite anode is attached to a stainless-steel electrode protruding from the top of the cell. Using an Autolab potentiostat attached to the stainless-steel electrodes, -2 V was applied to the membrane composite cathode and graphite anode. Permeate from the flow cell was collected in beakers stirred at 300 rpm over 10-minute intervals. At the end of each interval, the collected mass was weighed, and flux was calculated. Three 200 μL aliquots of permeate sample were taken at the end of each 10-minute interval to test the concentration of MO in that sample by the same method discussed for the batch system experiments.

4.2.6 Contact Angle Experiments

The contact angle of 0.25 mM MO droplets on the surface of 4 mg nZVI-CNT surface composite membranes was measured using an Optical Contact Angle device (OCA 35). These tests were completed to examine the wetting and electro-wetting characteristics of MO on the nZVI-CNT composite surface with and without an applied voltage. During electro-wetting tests, 2 V was applied to the surface through contact with the probes of a GW Instek GPS-1850D DC power supply.

4.3 Results and Discussion

4.3.1 nZVI-CNT Membrane Composite Morphology

The SEM image in Figure 4.2 shows a cross section of an nZVI-CNT membrane. Analyzing this image, and others taken on membrane samples of identical specifications, the average thickness of the 10 mg nZVI-CNT membrane surface composite was found to be approximately 6 μm.

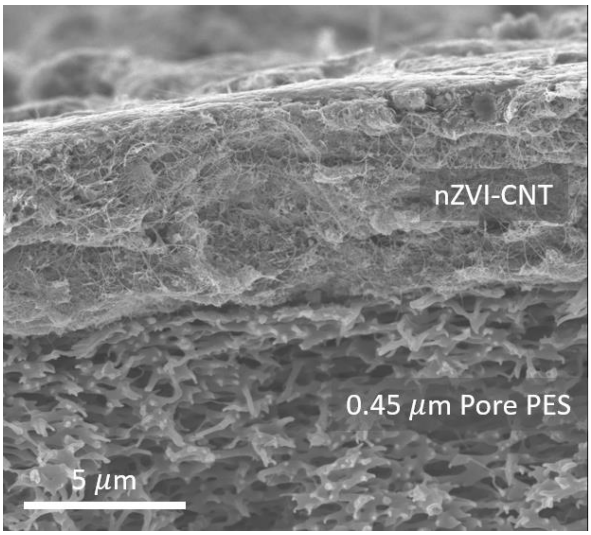

Figure 4.2. An SEM image of an nZVI-CNT membrane cross section at 5,000x magnification, showing both the thin film surface composite and the PES support membrane beneath it.

4.3.2 Catalytic Membrane Flux and Permeability

The pure water flux of membranes coated with 4 mg nZVI-CNT surface composites are shown in Figure 4.3, alongside the flux of a bare 0.45 μm pore size PES membrane which serves as a control.

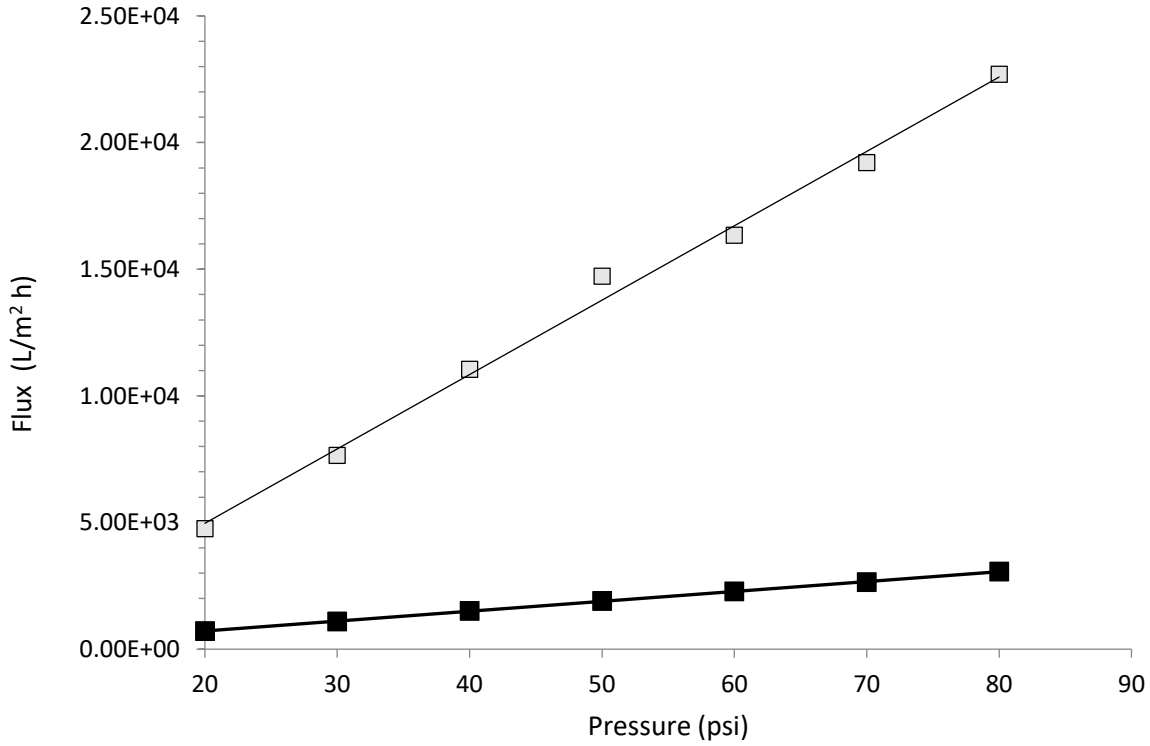

Figure 4.3. Pure water flux measurements for 0.45 μm pore size PES membranes (grey) and 0.45 μm pore size PES membranes with 4 mg of nZVI-CNT surface composites at 20-80 psi pressures.

Both the nZVI-CNT membranes and the PES support membranes show linear relationships between flux and applied pressure that is consistent with membrane theory [9]. Membrane permeabilities were obtained from the slopes corresponding to their flux vs. pressure data using linear regression. Calculated permeabilities indicate that membranes with 4 mg nZVI-CNT

composites are ~7.5 times less permeable than their PES support membranes alone, with permeabilities of 565.7 ± 8.0 L/m^{2}h·bar and 4258 ± 371.6 L/m^{2}h·bar respectively.

4.3.3 Continuous Removal of MO Using Catalytic Membranes

With the results of the batch system experiments having provided a proof-of-concept of the regenerative electro-catalytic performance of nZVI-CNT surface composite membranes, tests in a continuous system were carried out to determine the impact of flow through the catalytic membrane surfaces on reductive degradation efficacy. Figure 4.4 shows the mole % decrease in concentration between the MO in the feed and MO in the permeate, as well as volumetric flux for the continuous removal of 0.25 mM MO in a dead-end flow cell at 40 psi. These tests used nZVI-CNT surface composites as a cathode opposite a graphite anode with -2 V applied voltage. The results of the following three types of control experiments are also included in Figure 4.4 for comparison: systems without nZVI, without applied voltage, and without nZVI or applied voltage.

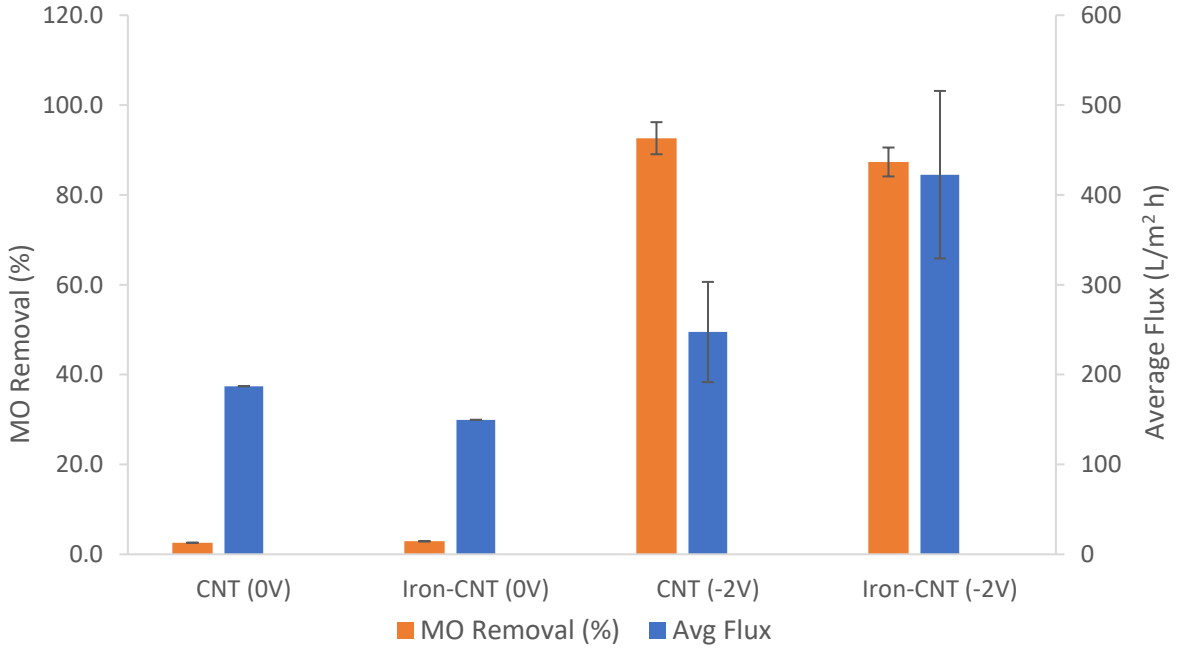

Figure 4.4. MO mole % Removed (orange) and Average Flux (blue) for dead-end continuous flow cell tests at 40 psi with various membrane surface composite cathode types and applied voltages. Error bars represent the 95% confidence interval on each set of triplicate tests.

Systems with nZVI-CNT composites operating at -2 V achieved 87.3 $\pm$ 3.2 % removal of MO on average. These results were closely comparable to those of control experiments lacking nZVI (92.6 $\pm$ 3.6%). It should be noted that within the 95% confidence interval there is no statistical difference between the mean percentage removal of MO by these systems. Control systems operating without applied voltage using nZVI-CNT and CNT composites achieved insignificant removal of MO and were closely comparable to one another (2.9% and 2.6% removal, respectively).

While systems with nZVI-CNT composites operating at -2 V and those without nZVI at -2 V achieved statistically similar MO removal, the nZVI-CNT membranes had significantly higher flux than the pure CNT membranes (422 $\pm$ 93.2 $\frac{\mathrm{L}}{\mathrm{m^2 h}}$, and 247 $\pm$ 55.8 $\frac{\mathrm{L}}{\mathrm{m^2 h}}$ respectively). With a greater transmembrane flux and the same MO removal, this suggests that systems with nZVI-CNT composite membranes degrade MO at a higher rate. Based on the time-dependent nature of the chemical reaction observed in the batch system experiments, it is logical to assume that a compromise exists between throughput (flux) and degradation (mole % of MO removed) in the system. A lower throughput enables a higher retention time of MO within the catalytic membrane, and thus greater contact time for degradation. Thus, the removal rate R, of MO is a more informative metric than mole % removal for describing a catalytic membrane's ability to remove contaminants in the permeate. The trade-off between throughput and degradation suggests that removal rate is the system's target objective to be maximized, as it is the product of throughput and contaminant concentration reduction. The removal rate R_i over any given time interval t_i is given by $R_i = (C_0 - C_i)\frac{V_i}{t_i}$, where V_i represents the permeate volume collected over the ith interval, and C_0 and C_i represent the molar concentrations (M) of the feed and the permeate collected over the ith interval, respectively. Figure 4.5 shows the average values for removal rates

over the course of continuous removal tests for the same experimental and control systems as outlined in Figure 4.4.

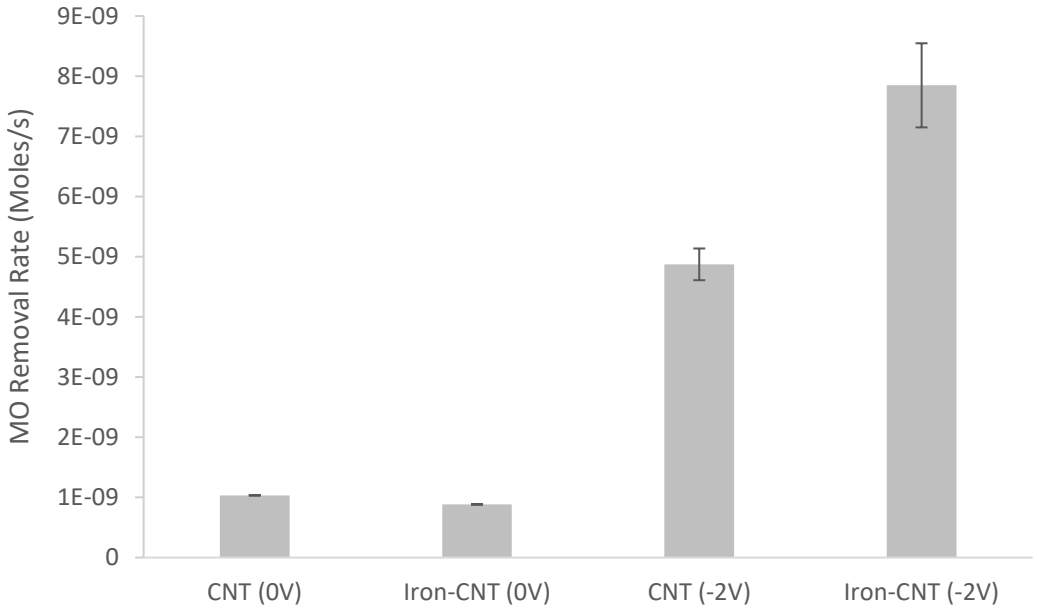

Figure 4.5. Removal rates for dead-end continuous flow cell tests with various membrane surface composite cathode types and applied voltages. Error bars represent the standard deviation across three triplicates.

Cross examining Figure 4.4 and 4.5, it is evident that although the systems using nZVI-CNT composites and those containing only CNTs show similar results in percent removal, the higher fluxes through the nZVI-CNT composites indicate that those systems are removing MO at a 1.6 times higher rate on average.

The results from Figure 4.5 also suggest that higher fluxes are achieved when a voltage is applied to the membrane surface composite. To investigate the effect of applied voltage on flux, an experiment was carried out in which a voltage was applied mid-test, and MO removal and flux were tracked throughout. Specifically, 0.25 mM MO was transported through nZVI-CNT

composite membranes under 40 psi with no applied voltage. After 30 minutes had elapsed, a -2 V voltage was applied to the nZVI-CNT membranes and the test was continued for two more hours. The flux and mole % removal throughout this test are presented in Figure 4.6.

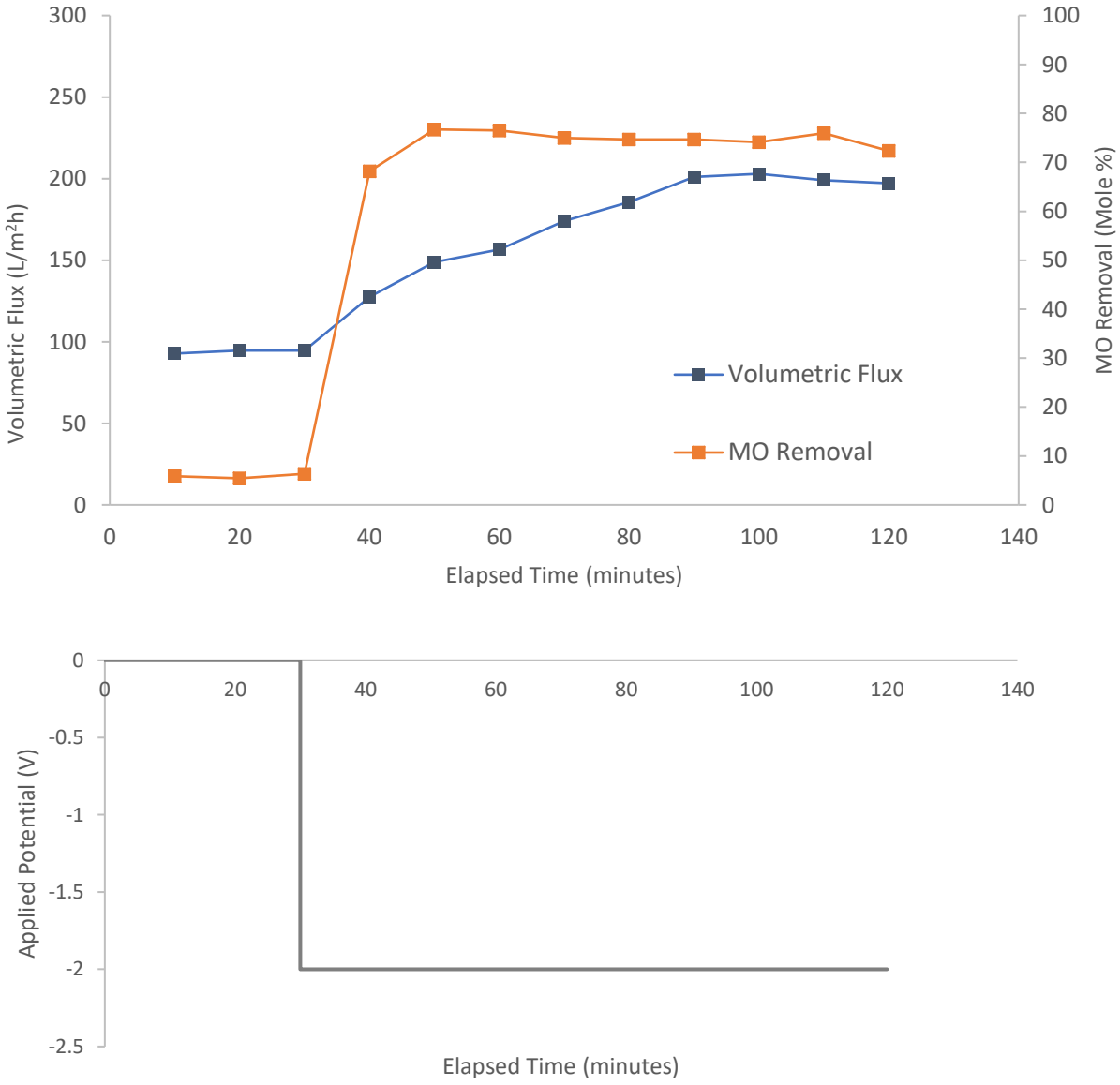

Figure 4.6. MO Mole % Removed (orange) and Average Flux (blue) for a dead-end continuous flow cell tests at 40 psi using an nZVI-CNT membrane composite cathode, in which a step change in applied voltage of 0 V to -2 V is made after 30 minutes elapsed.

From Figure 4.6, it is apparent that both MO removal and volumetric flux increased with the application of -2 V voltage. The response of flux to the step change in applied voltage appears similar to that of a first order response [137] and reached a steady state value nearly twice that at 0 V applied after approximately one hour. MO removal responded more rapidly to the step change in voltage, reaching a steady state (~76% moles removed) value after approximately 20 minutes (two sampling periods). Interestingly, the steady state flux achieved through the nZVI-CNT membrane composite post application of-2 V did not achieve the same flux as when the voltage was applied from the beginning of flux measurements.

Through a phenomenon known as electro-wetting, wetting of electrically conductive surfaces can be enhanced by inducing a charge on a capacitor or electrode in the presence of conductive liquids [131], [138]. Thus, it possible that the increased transmembrane flux was caused by enhanced adhesion forces of MO to the conductive surface composites when cathodic voltages were applied during membrane flux tests [131]. Contact angle experiments were carried out to investigate this effect using 0.25 mM droplets on an nZVI-CNT surface composite with and without an applied 2 V DC voltage. The observed contact angles were found to be $56.7 \pm 4.3°$ and $68.2 \pm 4.0°$ for surface composites with and without applied voltage, respectively, indicating that an applied voltage does encourage MO wetting. However, the 0.25 mM solution used in this study was prepared with DIW and therefore was not very conductive (~28 μS/m). As such, electro-wetting may not account for all the increased flux observed in the continuous MO removal experiments, and that other mechanisms may be at work, such as alterations to the CNT network under an applied voltage.

Removal rate, R, can also be used to compare the performance of the continuous and batch systems. However, since the batch system has no permeate volume collected over time, its rate of

removal is instead determined by $R(t) = \frac{dC(t)}{dt} V_{batch}$, where $C(t)$ represents the concentration of the batch as a function of time (modelled by linear-in-the-parameters regression), and V_{batch} represents the volume of the batch. As previously discussed, the concentration of a batch system as a function of time takes the form of $C(t) = 0.25e^{\alpha t}$, where $\alpha < 0$ and is representative of the system parameters. Thus, removal rate is a monotonically decreasing function of time, and the instantaneous removal rate, $R(0)$, can be used for establishing the maximum, most optimistic estimate of removal rate for comparison against the average removal rate of its continuous system counterpart. $C(t) = 0.25\mathrm{e}^{-0.023\mathrm{t}}$ represents the relationship of concentration over time for a nZVI-CNT composite cathode system operating at -2 V. The maximum, instantaneous rate of removal for that system is given by: $R(0) = \frac{dC(0)}{dt}(0.03\mathrm{L}) = 2.875 \times 10^{-9}$ moles/s. This removal rate is approximately 2.7 times less than that of its continuous counterpart, indicating that the continuous system is more effective than a batch system operating at its theoretical maximum MO removal rate. Additionally, the continuous system out-performs the batch system by achieving higher throughput. For instance, the continuous system can reduce the concentration of 30 mL of 0.25mM MO (the volume and molar concentration of the batch system) by ~87% in approximately 10-20 minutes, while the batch system requires approximately 90 minutes to achieve the same MO removal.

Further comparing the results of the batch and continuous systems, it may seem that the former possesses the advantage that it can continue in operation until a given batch of MO is completely removed, while the permeate MO concentration of the latter is constant and less than 100%. A two-factor design of experiments was devised to address this claim and investigate the manipulation of experimental factors on flux and MO removal. Concentration was chosen as a factor to investigate its effect on the kinetics of the reduction reaction to degrade MO, and the mass

transfer of MO to the membrane surface. Pressure was chosen as a second factor to manipulate flow rate through the cell, and thus the retention time of the MO feed. The DOE experimental factors and corresponding results are shown below in Table 4.1.

Table 4.1 Structure and results of a design of experiments investigating the effects of feed concentration and pressure on the flux and mole % removal of continuous tests using a system operating at -2 V with an nZVI-CNT cathode, as well as the results of triplicate tests previously discussed for comparison (blue).

Experiment Number	Order Tested	MO Concentration (mM)	Feed Pressure (psi)	Flux (L/m^2h)	MO Removal (Mole %)	Removal Rate (Moles/s $\times 10^9$)
1	4	0.125	20	229	93.6	2.26
2	2	0.25	20	280	89.5	5.35
3	3	0.125	80	485	65.0	3.30
4	1	0.25	80	505	72.3	7.56
N/A	N/A	0.25	40	422	87.3	7.85

The results of this DOE confirm the compromise between flux and the extent to which the concentration of the MO feed is degraded. Compared to the nZVI-CNT/-2 V/0.25 mM/40 psi tests previously discussed (87.3% removal, as shown in blue in Table 4.1), tests at lower pressures (20 psi) and thus lower flux achieve slightly higher removal (89.5%), and tests at higher pressures (80 psi) and thus higher flux, achieve significantly less removal (72.3%). The results of this DOE also indicate that the concentration of the MO feed has a limited effect in the flux and mole % removal in a continuous system. Thus, if mole % removal remains constant regardless of the feed

concentration, a second pass of MO through a system operating at 80 psi would likely achieve similar results (92.3 mole % removed) to a single pass of a system operating at 20 psi (89.5 mole % removed).

Finally, the results of Experiment 4 in the DOE (0.25 mM, 80 psi) illustrate the point that suitable constraints must be considered when using removal rate as a metric of system performance. Since removal rate is the product of volumetric flow rate and change in concentration, Experiment 4 yielded a high removal rate due to its high flux through the membrane despite its relatively poor decrease in MO concentration (72.3% removal). Removal rate is a pragmatic metric for benchmarking system performance because it encapsulates information about both flux and mole % removal. Thus, minimum constraints must be applied on those outputs when seeking to maximize removal rate to avoid sacrificing either output at the expense of the other.

4.4 Conclusions

The membranes with nZVI-CNT composites achieved ~87% molar removal of MO feed in a single pass through a continuous dead-end flow cell operated at -2 V and 40 psi. The average rate of removal of the continuous system was found to outperform the instantaneous (maximum) rate of removal of its batch system counterpart by 2.7 times. The application of a negative voltage to the nZVI-CNT composite cathode caused an increase in the transmembrane flux due to electro-wetting. The concentration of the MO feed in a continuous system appears to have little effect on that system's removal rate. The pressure of the feed, however, has a significant effect on the flux, as pressure controls the retention time of MO within the membrane, and thereby the MO removal rate, and the total MO mole % removal.

Chapter 5

Statistical Modelling and Optimization of the Batch Removal Performance of Catalytic Membranes using Latent Variable Methods

Abstract

Chlorinated organic compounds and azo dyes represent challenging contaminants in modern wastewater treatment. We developed electro-catalytic membrane surface composites composed of carbon nanotubes (CNTs) and nano zero-valent iron (nZVI) particles to treat these contaminants. 41 membranes with varying synthesis parameters were produced and tested in an electrochemical cell to evaluate the impact of seven experimental variables in chemically reducing methyl orange (MO) dye over a 60-minute period. An electrochemical cell was formed from the iron nanoparticle-CNT catalytic membrane composite as the cathode, and a graphite foil strip as the anode, in an MO electrolyte. Partial least squares regression (PLSR) was used to develop a model relating the membrane characteristics and experimental parameters to the removal of MO over time. The importance and effect of each parameter on MO removal was evaluated. The validated PLSR model was used to solve for an optimum set of membrane and experimental parameters to achieve maximum MO removal. The MO removal under predicted optimum conditions closely matched experimental data and achieved approximately 255% more removal than that of tests based on a priori chosen parameters. Finally, an Auto-regression partial least squares (ARPLS) model was developed to predict MO removal timeseries data beyond the experimentally evaluated 60-minute test window.

5.1 Introduction

Partial least squares regression (or projection to latent structures regression, PLSR) is a data driven method for relating input and output data matrices to derive a multivariate linear model [139]. A PLSR model takes a data set with N observations of K number of variables (dimensions) and captures the variation in the data by projecting that system into a reduced dimensional space of A components. This reduced set of components ($A < K$) is essentially the collection of hidden (but physically meaningless) variables within the data that encapsulate its variation and are thus termed "latent variables". Latent variables are useful for both an analysis of the relationship between the input and output data matrices, and for quantitative predictions of the outputs given a new set of input observations [139], [140].

Previous work in Chapter 3 has demonstrated the enhanced electro-catalytic batch removal of methyl orange dye using nZVI-CNT surface composite membrane cathodes alongside a graphite anode. Having validated this concept, it is desirable to investigate the effects of each of the seven experimental parameters in the batch system (listed in Table 5.1) to model and optimize azo dye removal performance. In this study, a Partial Least Squares (or Projection to Latent Structures) regression (PLSR) model was developed to accomplish these objectives.

5.2 Materials and Methods

5.2.1 Materials

All the solutions used for synthesis, characterization, and testing were prepared in de-ionized water from a Sartorious Arium Mini device. Single/double walled COOH-functionalized carbon nanotubes (1-4 nm diameter, 5-30 μm length, 2.73 wt% functional content) were purchased from Cheaptubes. The following chemicals used were all of lab grade purity (> 98% pure). Iron

sulfate pentahydrate was purchased from Sigma Aldrich. Sodium borohydride was purchased from Alfa Aesar. Sodium dodecyl sulfate was purchased from Anachemia.

All nitrogen gas used came from Air Liquide compressed nitrogen tanks (100% pure). The circular flat sheet polyether sulfone ultrafiltration membranes were purchased from Sterlitech (0.45 μm pore size, 47 mm diameter). Methyl orange powder was purchased from Sigma Aldrich.

5.2.2 Catalytic Membrane Composite Fabrication with Varying Parameters

The procedure for developing the catalytic nZVI-CNT surface composites used in this study built upon the both the procedural foundations established in Section 3.2.2 and the alterations to that procedure discussed in Section 4.2.2. Namely the synthesis parameters for the membrane composites developed in this study were varied for the purpose of understanding their effect on contaminant removal through subsequent modelling. The mass of the nZVI-CNT surface composite varied between 5 – 10 mg, and the ratio of SDS surfactant used for CNT dispersion varied between 1:1 and 1:1.5 mg of CNT: mg of SDS.

5.2.3 Methyl Orange Batch Removal Experiments

A batch test system was devised to test the performance of nZVI-CNT membranes in removing contaminants under varying experimental parameters. The azo dye, methyl orange (MO), was chosen as a model contaminant so that UV-Vis-measured dye intensity (absorbance) data could be correlated to dye concentration via a calibration curve (Figure S1). This calibration curve was used to calculate the concentration of samples obtained over the course of a batch test. Figure 5.1 shows a schematic of the experimental design, in which a conductive membrane and a graphite strip are hung as electrodes in a batch of 0.25mM MO dye. A voltage is applied between

the catalytic membrane cathode, and the graphite strip anode, to form an electrochemical cell that facilitates the degradation of the 0.25 mM MO dye batch.

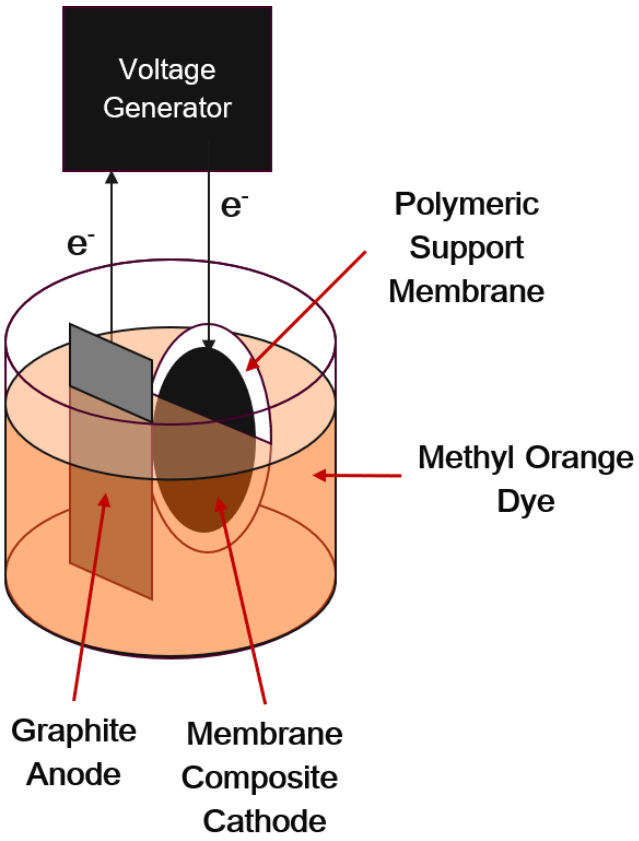

Figure 5.1. A schematic of the MO batch removal experiments, in which voltage is supplied to the surface of the composite cathode, and a graphite strip anode.

200 µL samples are taken from the well mixed batch (stirring at 900 rpm) at 10-minute intervals. The absorbances for these samples are then measured at 464 nm using a Tecan Spark UV Vis Spectrophotometer and Figure S1 is used to calculate the corresponding concentration and moles degraded. The experimental parameters varied are listed below in Table 5.1.

Table 5.1. Experimental parameters for electrochemical batch removal tests using catalytic nZVI-CNT membrane surface composites.

Experimental Parameters	Range	Units
Batch Concentration	0.025 – 0.25	Millimolar (mM)
Applied Voltage	-2 – 0	Volts (V)
Electrode Spacing	0.3 – 2	Centimeters (cm)
Iron Content	0 – 1.07	Mass (mg)
CNT Content	0 – 10	Mass (mg)
Surfactant Ratio	1:0 – 1:1.5	mg CNTs: mg SDS
Batch Volume	0.03 – 0.1	Litres (L)

5.2.4 Modelling Batch Removal Over Time Using PLSR

Using data from 41 batch MO removal experiments, a PLSR model was developed in Aspen Plus ProMV to relate the seven experimental inputs to seven outcome variables. These seven outcome variables are the moles removed from the system at seven 10-minute time increments up to one hour, as shown in Table 5.2.

Table 5.2. Input and output variables used to construct a PLSR Model on the batch removal system.

Input Variables	Output Variables	
Batch Concentration	Moles MO removed at:	0 minutes
Applied Voltage		10 minutes
Electrode Spacing		20 minutes
Iron Content		30 minutes
CNT Content		40 minutes
Surfactant Ratio		50 minutes
Batch Volume		60 minutes

It is important to note that the outcome variables are expected to be highly correlated with one another since moles removed is a cumulative measurement. The number of moles removed at any given time-step includes the number of moles removed in the last 10 minutes as well as at all previous time increments. This would be a problem for methods such as multiple linear regression, however a PLSR model does not rely on the assumption of independence between its parameters and is thus equipped to handle such highly correlative output data [139].

The structure of a generic PLSR Model is visually described by Figure 5.2, and Table 5.3 serves to clarify and summarize the purpose of each of the blocks in the model [139]. The magnitude and sign of the input weights W in relation to the output weights C provides insight as to how each experimental parameter affects removal performance.

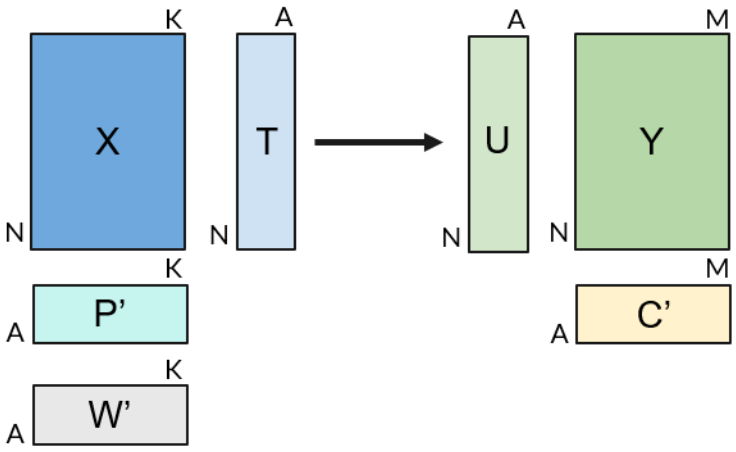

Figure 5.2. A structural visualization of the matrix blocks used in a PLSR model.

Table 5.3. Definitions, dimensions, and indices for the matrix blocks in a PLSR model. Note that W', C', and P' denote the transposes of the W, C, and P matrices respectively.

Dimensions	Index	Definition
A	a	The total number of components in the PLS Model
K	k	The total number of input variables in the PLS Model
M	m	The total number of components in the PLS Model
N	i	The total number of observations used in the PLS Model
Matrix	**Dimensions**	**Definition**
X	N x K	Input data with N # of observations of K # of variables
Y	N x M	Output data with N # of observations of M # of variables
T	N x A	Input scores with N # of observations of A # of components
U	N x A	Output scores with N # of observations of A # of components
W	K x A	Input weights for K # of variables corresponding to A # of components, which can be used to calculate T given X: $T = XW$
C	M x A	Output weights for M # of variables corresponding to A # of components, which can be used to predict Y given T: $\hat{Y} = TC'$
P	K x A	The loading matrix for the PLSR Model, which can be used to predict Y given X and T: $\hat{X} = TP'$

5.2.5 Using PLSR to Predict Optimal Batch Removal Performance

Aspen Plus ProMV software was used to conduct an optimization using the model developed. The objective of the optimization was to maximize MO removal achieved by the completion of the test (i.e. MO moles removed at 60 minutes). Constraints were placed on each of the input decision variables so that the software would reach a solution that was experimentally feasible. These experimental constraints are listed in Table 5.4.

Table 5.4. Input decision variable constraints for optimizing the batch removal of MO at 60 min.

Experimental Parameters	Lower Constraint	Upper Constraint
Batch Concentration (mM)	0.025	0.25
Applied Voltage (V)	---	0
Electrode Spacing (cm)	0.03	---
Iron Content (mg)	0	---
CNT Content (mg)	0	---
Surfactant Ratio	1.1	---
Batch Volume (L)	0.03	---

Note that while some of the observations used to construct this model had surfactant ratios of 1 mg CNTs: 0 mg SDS surfactant, a minimum constraint of 1 mg CNTs: 1 mg SDS is specified in the optimization formulation. A non-zero mass of SDS is a necessary experimental parameter for synthesizing uniform nZVI-CNT membrane coatings. A lack of surfactant – and thus a lack of membrane surface uniformity– is acceptable for batch removal tests since flow through the membrane was not examined in this study. However, for continuous trans-membrane contaminant degradation, a minimum amount of surfactant is required to ensure a uniform membrane composite thickness. Composite uniformity ensures repeatable trans-membrane fluxes of contaminants. Thus minimum non-zero constraints were placed on surfactant ratio to ensure that this model would reach optimization result that was useful for future continuous systems analysis.

After solving for the optimum experimental parameters, a test was carried out with the corresponding optimal decision variables to compare how the maximized MO removal performance predicted by the software compared to an experimentally measured value.

5.2.6 Projecting Batch Removal Performance Using Auto-Regression PLS

Auto-Regression Partial Least Squares (ARPLS) was implemented to predict data in the optimal batch removal timeseries beyond the experimentally observed data. ARPLS uses repeatedly forward shifted timeseries data to create a set of input variables at future times. Each variable created at a subsequent time step uses the timeseries data shifted forward by one observation. The variable columns created by these shifts are called a lags [141]. The ensemble of lagged variables forms a block of input data that can be provided to a PLSR model to predict the next point in the timeseries.

In this study, an ARPLS model was generated using input data blocks of nine observations and six variables ($K = 6$, one for each lag from 0 to 5) to describe the timeseries data of optimal removal performance. After constructing the model, an investigation of the loading plot for component 1 showed that each of the lags used in the model made a significant contribution. As such, none of these lags were excluded in subsequent analysis. The model was first validated by using it to predict MO removal for all time increments between 150 – 180 min inclusive and comparing these predicted values to those observed in experimental testing under the same conditions. Then the validated model was used to predict batch removal values for ten time increments beyond those measured experimentally. Estimates of the error in these predictions were determined and are further discussed in Section 5.5.

5.3 Results & Discussion

5.3.1 Modelling Batch Removal Over Time Using PLS

A two-component PLSR model was used to describe the relationship between the experimental input parameters X and the MO removal at different time increments Y. This means that the seven variables in the system were projected onto a space with two latent variables that best capture the variability in the data. Figure 5.3 shows a summary of the cumulative R^2 and Q^2 values attained with the addition of components 1 and 2.

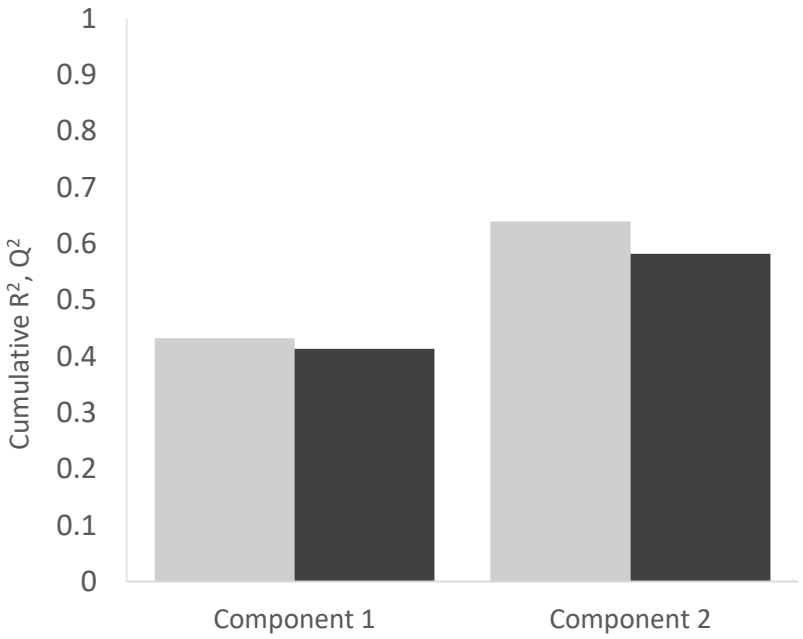

Figure 5.3. Cumulative R^2 (gray), and cumulative Q^2 (black) attained by a PLSR model with the addition of a first and second component fit to the MO batch removal experiment data.

Additional components were not kept in the model, as their addition raised only the cumulative R^2 with no change to the cumulative Q^2. This is an indication that adding more

components would overfit the model, increasing the accuracy with which it predicts the training data used to make it, but lowering its predictive power for use with future observations due to overfitting [139]. Figure 5.3 shows that two components yield a model with an R^2 of 0.64 and a Q^2 of 0.58, which indicates a respectable degree of predictive power [139].

The weights for the input and output variables with respect to the first component (W_1 and C_1 respectively) are shown in a bar plot given by Figure 5.4. As previously explained, the output variable weights for the removal of MO at different time increments are highly correlated with one another.

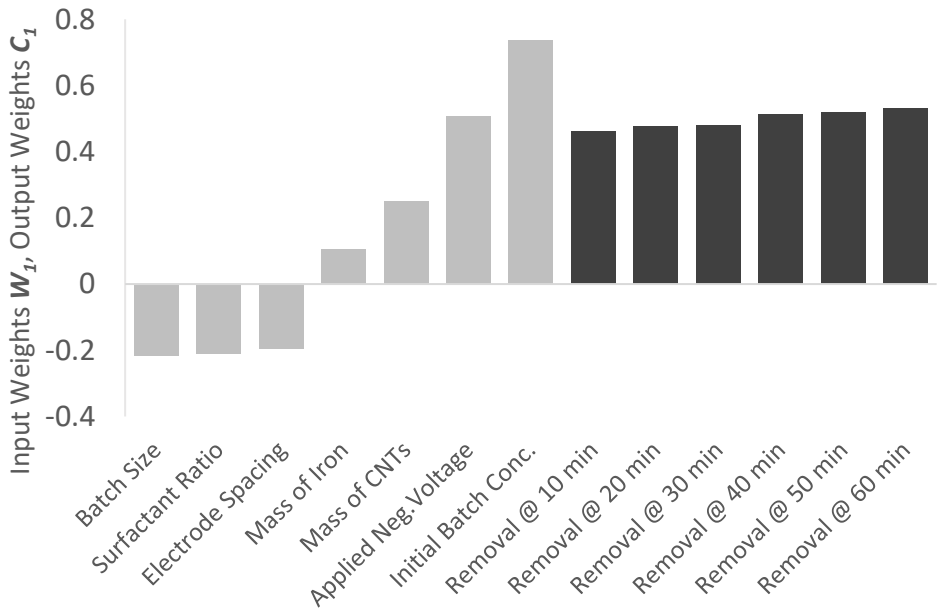

Figure 5.4. Input weights W_1 (gray) and output weights C_1 (black) for the first component of a PLS model fit to the MO batch removal experiment data.

Based on the input weights relative to the determined output weights, the PLSR model suggests that initial batch concentration, negative applied voltage, mass of CNTs in the membrane

composite, and mass of iron in the membrane composite are correlated with increasing batch removal. By the same analysis batch size, surfactant ratio, and electrode spacing are anti-correlated with increasing batch removal.

Of the seven input variables, batch concentration possesses the strongest positive correlation with MO removal. The magnitude of its weight in the model therefore suggests that the rate of MO removal by electrochemical reduction and adsorption is highly dependent on its concentration. This indicates that the mass transfer of MO molecules to the surface of the membrane cathode is a limiting factor to its removal, which is substantiated by prior work and theoretical models for unsteady state diffusion and reaction based on Fick's law [9], [98]. This could be problematic for practical applications, as COCs and azo dyes are often found in trace levels of contamination (ppm concentrations) [32].

The correlation of the mass of CNTs and iron mean that both materials are important for facilitating the reduction of adsorption of MO. This finding is substantiated by previous work, as increasing the mass of those materials in the membrane surface composite increases its surface area and thus the sites available for reaction and adsorption [25], [26], [29], [32], [34], [35], [38], [49], [124]. The CNTs' performance as an adsorbent and electrode for the electrochemical reduction of azo dyes is well known. Distinguishing the mechanism of nZVI removal of azo dyes that is positively correlated to azo dye removal is more challenging. We hypothesize two separate mechanisms: 1) the applied voltage to the membrane composite regenerates the reactivity of the embedded iron nanoparticles, reducing them back to a zero-valent state such that they can continually reduce MO molecules and electro-catalytically remove them from solution; and 2) the iron acts as an additional adsorbent and electrical conductor for electrochemical degradation of MO. Further experiments and controls are required to explain this correlation, such as X-ray

photoelectron spectroscopy (XPS) and the development of an adsorption isotherm. XPS could be used to examine the electrochemical state of the iron in the membrane surface composite and confirm whether it has been chemically reduced back to nZVI. An adsorption isotherm using nZVI-CNT surface composite membranes and MO as the adsorbent and adsorbate respectively would help in deconvoluting the contributions made to MO removal by adsorption and reaction.

Figure 5.4 implies that applying negative cathodic voltages to the membrane surface composite increases MO removal. An increase in the voltage magnitude may speed up the kinetics of the reduction reaction, or it may accelerate the iron particle regeneration. Additionally, charged electrodes in an oxygenated aqueous medium can produce hydrogen peroxide, a strong reducing agent that could be contributing to the removal of MO via a mediated reduction mechanism [142], [143].

Referring again to Figure 5.4, batch size, the mass ratio of surfactants to CNTs, and electrode spacing are anti-correlated to performance to roughly the same degree. It is intuitive that increasing surfactant ratio has a negative effect on removal. SDS stabilizes hydrophobic CNTs in an aqueous environment by wrapping around them to minimize interactions with water. Surfactant wrapping of CNTs reduces their contact with each other in the membrane surface composite network. This lowers the conductivity of the composite and thus its performance as an electrode and as a scaffold with which to pass electrons to regenerate the reactivity of the iron particles. In addition, wrapping CNTs with SDS blocks surface sites for the nucleation of nZVI particles during membrane composite fabrication, and blocks potential sites for reaction during testing. The anti-correlation of electrode spacing with MO removal is a result of the weakening of the electric field between the electrodes with increasing distance. Finally, the anti-correlation between batch size and MO removal is likely due to the experimental setup, i.e. that the same stirring apparatus and

speed (900 rpm) were used for all tests. Assuming the rate of removal is mass transfer limited, larger batches will be stirred less effectively than smaller ones, lowering the rate of convective mass transfer to the membrane composite surface [9].

5.3.2 Using PLS to Predict Optimal Batch Removal Performance

Having run the optimization problem previously outlined in section 5.3.2, maximized MO removal values were predicted by the PLSR model for the optimum set of input parameters. Of the constraints placed upon the optimization, only those for batch concentration (maximum of 0.25 mM) and surfactant ratio (minimum ratio of 1 mg SDS:1 mg CNTs) were active at the solution to the optimization problem. A constraint is considered active when the solver used to carry out the optimization finds that the optimal value for its corresponding decision variable exists at a limit posed by that constraint. An experiment was carried out using those same optimal parameters for comparison and validation of the model. The MO removal results predicted by the PLSR model, and those determined experimentally are included in Table 5.5.

Table 5.5. Results for the predicted and observed values of optimum MO removal. The decision variables at the optimum and the constraints they are subject to are also shown.

Experimental Parameters	Lower Constraint	Upper Constraint	Optimum	Time Interval (min)	Predicted Removal (μmoles)	Observed Removal (μmoles)
Batch Concentration (mM)	0.025	0.25	0.25	0	0	0
Applied Voltage (V)	---	0	-3.2	10	1.84	1.79
Electrode Spacing (cm)	0.03	---	1.3	20	2.87	2.89
Iron Content (mg)	0	---	~1.0	30	3.72	4.26
CNT Content (mg)	0	---	~10	40	4.69	5.09
Surfactant Ratio	1.1	---	1:1	50	5.29	5.62
Batch Volume (L)	0.03	---	0.09	60	5.89	6.05

While the experimentally observed MO removal values from the test carried out with optimal parameters slightly out-perform the predictions made by the PLS model at the optimum, the maximum deviation of the predicted data from the observed data was ~14.3% (occurring at an elapsed time of 30 minutes), which speaks to the similarity of the data.

The model's success in predicting the optimum membrane performance highlights the benefits of this optimization. Figure 5.5 shows the observed vs. predicted MO removal at the optimum experimental parameters in relation to experimental trials whose parameters lie within the feasible solution space of the optimization (i.e. within the constraints imposed on the optimization decision variables).

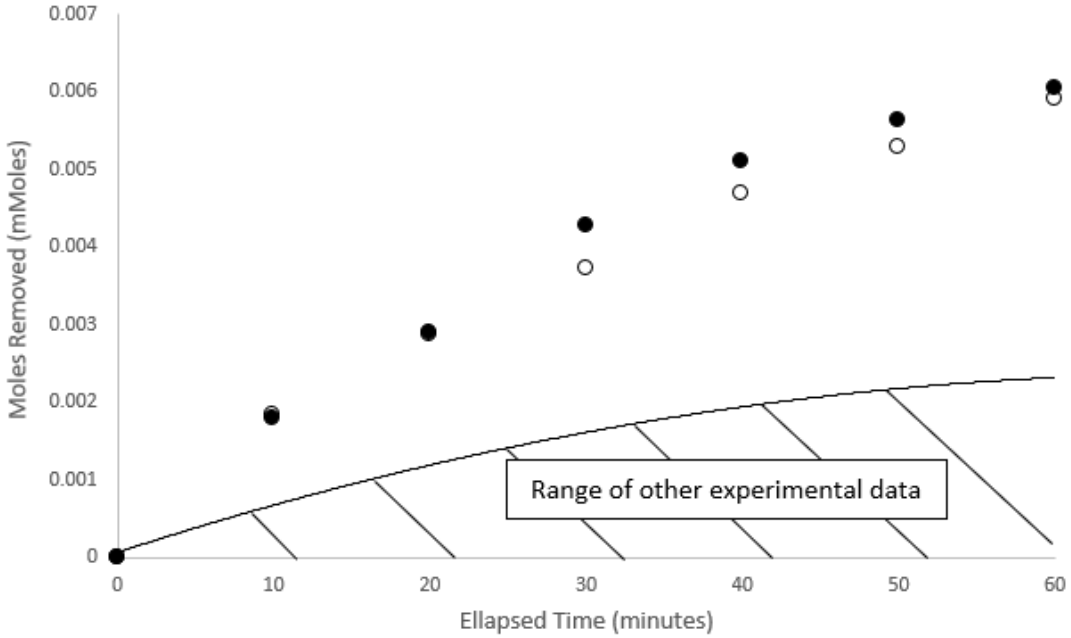

Figure 5.5. Observed (black circles) vs. predicted (white circles) values for MO removal at optimal experimental parameters, as determined by the PLS model. The range of other experimental tests is shown for comparison.

As seen in Figure 5.5, it is evident that the model is not only accurate in predicting MO removal, but also successful in determining a set of experimental parameters that substantially improved MO removal; the test performance of at the optimum surpassed that of the next highest-performing observation by 255%.

5.3.3 Projecting Batch Removal Performance Using Auto-Regression PLS

An ARPLS model with 5 lags and one component ($R^2 = 0.98, Q^2 = 0.98$) was fit to describe the timeseries data for MO removal using the optimum conditions explored in section 5.3.2. Unlike previous experiments, the batch test carried out under optimum conditions proceeded for 210 minutes (3.5 hours) to collect a suitable number of observations for this analysis. The goal

of this model was to predict timeseries data beyond those experimentally measured to determine the amount of time required to completely degrade the MO batch. Figure 5.6 shows an observed vs. predicted plot used to validate the performance of the ARPLS model. This figure compares predictions made for time increments between and including 150-210 minutes to experimental data at those same times.

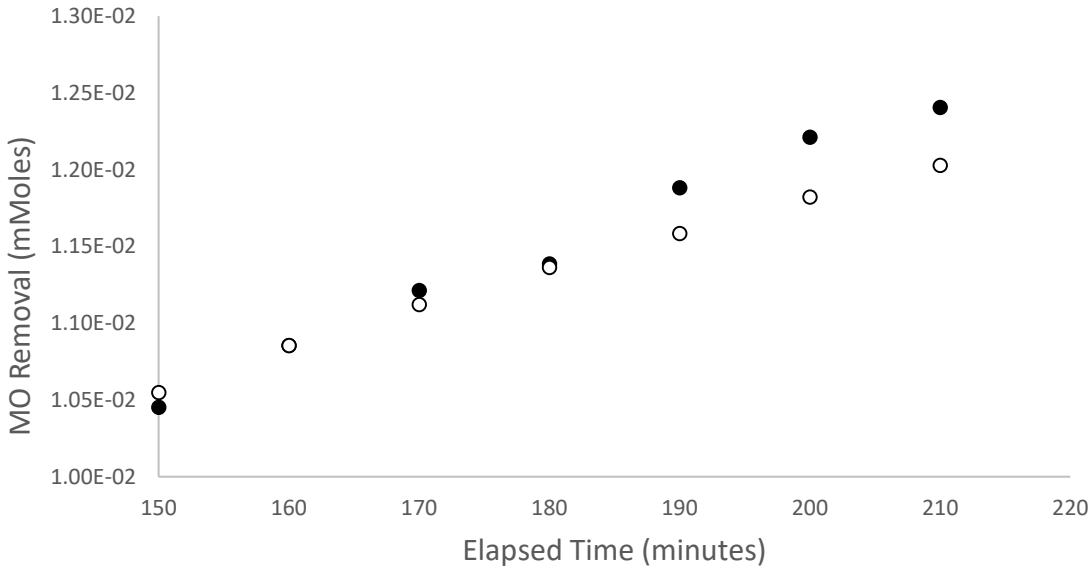

Figure 5.6. An observed (black circles) vs. predicted (white circles) plot used to validate the accuracy of the ARPLS model created on the optimum RO removal timeseries data.

The trajectory of the observed values is steeper than those predicted by the ARPLS model, thus the two series diverge overtime. As expected with an auto-regressive method, the accuracy of the prediction decreases with each successive time step, as each prediction adds to the cumulative error of all those before it.

Figure 5.7 shows the application of the ARPLS model to predict MO removal for ten time-increments from 210 minutes to 310 minutes, as well as the experimental observations preceding those predictions.

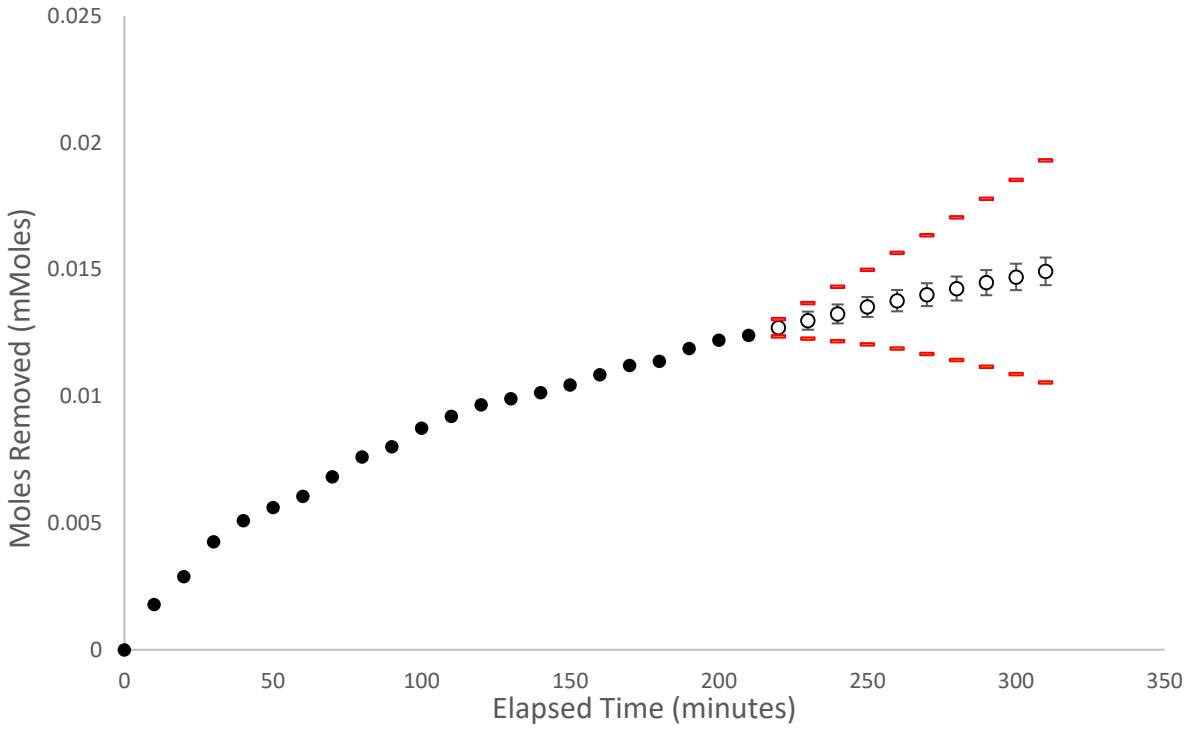

Figure 5.7. A timeseries plot of observed experimental values (black circles) for MO removal using optimal parameters, extended using predictions made by the ARPLS model (white circles). Error bars on the predictions come from 95% prediction intervals, and the red represent the cumulative prediction intervals.

From Figure 5.7, the values predicted using the ARPLS model appear to match the trajectory of the data, with relatively small error as indicated by the prediction intervals. However, the error in the model predictions compounds with every time step. Upper and lower conservative estimates of this compounded error are shown by the red bars on Figure 5.7. Thus, this model

succeeds in making accurate predictions approximately 30 to 50 minutes into the future but would likely fail in accurately predicting the time required to remove all the MO from the system due to the compounding error added with each prediction.

5.4 Conclusions and Future Work

In this study a PLSR model was used to examine the effects of experimental parameters on the removal of methyl orange from a batch system with electro-catalytic nZVI-CNT surface composite membranes. In order of decreasing importance, initial batch concentration, negative applied voltage, mass of CNTs forming the thin film network, and the mass of nZVI embedded in the network were all found to be positively correlated with MO removal. Conversely, electrode spacing, surfactant ratio, and batch size were all found to be anti-correlated with MO removal. A constrained optimization to maximize MO removal was successfully implemented and predictions were validated with experimental results. The MO removal operating at these optimal conditions was found to be 255% greater than the next highest performing observation within the feasible set. Finally, experimental data for MO removal using the optimal parameters over a 3.5-hour period was modelled with ARPLS. The model proved accurate enough to predict MO removal 30 to 50 minutes into the future beyond experimentally collected data.

Chapter 6

Conclusions and Future Work

6.1 Conclusions

The focus of this project was to develop permeable, electrically conductive, electrochemically reactive membrane surface composites capable of facilitating the enhanced electro-catalytic degradation of azo dyes in solution. SEM and TEM images have shown that nZVI can be grown and stabilized in a network of functionalized CNTs. ICP-OES and 4-point probe conductivity tests results confirm that this network can be filter deposited into a conductive thin film on the surface of a polymeric support membrane without the loss of iron. The results of batch system tests indicate a synergistic enhancement of dye removal is achieved by adding nZVI and a negative voltage to the membrane surface composite, as compared to controls. This enhanced dye removal could be caused by electro-catalytic reactivity supplied by nZVI reactivity regenerated through the application negative cathodic voltages. It is also possible that the enhanced reactivity of the solution is caused by electro-Fenton chemistry, however, such an effect would be more significant at pH values lower than the neutral pH at which these tests were conducted.

A statistical analysis of batch system test results using a PLSR model constructed with two components showed that the following parameters were positively correlated with increased MO removal in order of decreasing importance: initial batch concentration, applied negative voltage, mass of CNTs composing the surface composite thin film, and mass of iron embedded in the surface composite thin film. Conversely, the model found the following parameters (in order of decreasing importance) to be anti-correlated with batch removal: batch size, surfactant ratio, and electrode spacing. An optimization of these batch system parameters yielded a timeseries of

expected removal results 255% higher (after 60 minutes) than any of the experiments with parameters in the feasible set formed by the constraints specified in the optimization formulation. The model and its optimization result were validated by conducting a batch test using the optimal set of experimental parameters. The observed timeseries results of this experiment closely matched those predicted by the model at the optimum, with a maximum deviation of ~14.3% between any pair of values in the observed vs. predicted timeseries.

nZVI-CNT membranes with 4 mg of surface composite mass were employed to remove MO in a continuous system utilizing an electrochemical dead-end flow cell. Approximately 87 mole % removal of MO was achieved in the permeate of systems operating at 40 psi with -2 V voltage applied to the nZVI-CNT surface composite cathode opposite a graphite anode. The average rate of permeate flux across the nZVI-CNT surface composite membrane at 40 psi was 422 ± 93.2 L/m^{2}h. While nZVI-CNT surface composite systems achieved similar MO permeate concentrations to those using CNT membrane composites with no nZVI, the transmembrane flux at 40 psi through the former system type was on average ~1.7 times greater than those achieved by the latter. As such, nZVI-CNT surface composite cathode systems at 40 psi and -2 V removed MO at a rate ~1.6 times greater than those using CNT surface composite cathodes.

It was observed that a step change of 0 to -2 V applied to a continuous system using an nZVI-CNT cathode approximately doubled the transmembrane flux (from 94.1 ± 4.00 L/m^{2}h to 199 ± 5.81 L/m^{2}h). Based on relevant theory [131], [138] and the results of contact angle experiments showing increased wetting of MO with a 2 V applied voltage to an nZVI-CNT membrane surface composite, it is likely that this observed increase in flux is due to electro-wetting.

The results of a design of experiments varying the concentration of the MO feed and the feed pressure in a continuous dead-end electrochemical system using nZVI-CNT cathodes with -2 V applied confirmed that a compromise exists between throughput (transmembrane flux) and effluent quality (decrease in MO permeate concentration). Increasing the MO feed pressure resulted in higher fluxes, but at the expense of relatively increased MO permeate concentrations. Conversely, lower MO feed pressures result in slightly lower MO permeate concentrations but result in a much lower transmembrane flux through the system. Contrary to the results of the batch system modelling discussed in Section 5.3.1 – which indicated that MO batch concentration had a strong correlation with MO removal over time – the concentration of the MO feed to the electrochemical continuous tests had an insignificant effect on MO permeate concentration. Flux was similarly unaffected by MO feed concentration. Since direct reduction of MO at the surface composite cathode is primarily responsible for its removal from the system, it is likely that this discrepancy in the importance of MO feed concentration to the batch and continuous systems can be explained by the differences in the mass transfer of MO to the cathode. In the batch system, MO dye comes into contact with the cathode through solution diffusion and convective mass transfer driven by stirring, both of which are directly proportional to dye concentration [9]. In the continuous system, however, the pressure applied to the feed drives the mass transfer of MO to the cathode's surface, and therefore the role of concentration in encouraging MO diffusion to the cathode is less important.

Finally, comparing the average removal rate of the continuous system to the maximum (instantaneous) removal rate of the batch system, it is apparent that the former removes MO feed 2.7 times faster. Furthermore, the continuous system demonstrates higher throughput than the batch system. A continuous system operating at 40 psi using an nZVI-CNT cathode with -2 V

applied can remediate a 30 mL 0.25 mM MO feed by 87 mole % in 10-20 minutes, while a batch system with identical specifications (excluding the applied pressure) achieves that same molar removal within approximately 90 minutes (1.5 hours).

6.2 Future Work and Recommendations

Further studies and experiments are required to understand the adsorptive capacities of the membrane surface composites and distinguish the effects of adsorption and degradation on MO removal. This can be accomplished by conducting multiple batch tests using nZVI-CNT surface composite membranes without a graphite electrode or an applied voltage, in which the steady state removal of MO at various concentrations is determined to construct an adsorption isotherm.

A variety of experiments could be conducted to further analyze the performance of nZVI-CNT surface composites in a continuous system. The PLSR model for the batch system discussed in Chapter 5 indicates that the more negative voltages applied to the cathode result in increased MO removal. Continuous removal experiments at varying potentials would yield a greater understanding of the relationship between MO removal and increasingly greater magnitudes of applied negative voltage. If there are diminishing returns on MO removal at increasingly negative potentials, these experiments could serve in determining an optimal operating voltage. Furthermore, since various potentials will have different effects on electrochemical MO degradation through direct reduction at the CNT cathode, regeneration of nZVI, and ROS generation, a larger range of voltages will help to examine how these mechanisms contribute to MO Removal. In these experiments, the flow cell would ideally be retrofit with a dissolved oxygen probe to continuously monitor the concentration of ROS in solution and its contribution to MO degradation.

Additionally, experiments with multiple dead-end flow cells in series with different feed concentration would help to better understand the capabilities and kinetics of MO degradation in a continuous system. This could be accomplished by using permeate from one continuous removal test as the feed for a second test using the same cell but cleaned and with a different nZVI-CNT surface composite membrane.

While the decolourization of MO indicates its degradation, the substituents of that reaction must still be considered if this technology is to ever be used on a larger scale. Thus, tests analyzing the total organic carbon present in permeate samples should be completed in subsequent continuous removal tests to determine whether or not this technology can meet environmental standards of chemical oxygen demand (COD).

If this technology is developed and optimized further, the nZVI-CNT composite membrane system discussed in this thesis would be best utilized in textile industry outlets and pump-and-treat processes for azo dyes and COCs respectively. Textile industry effluents typically possess azo dyes in concentrations between 50 and 100 ppm and have few other constituents [134]. Thus nZVI-CNT membrane modules could be easily retrofitted on the tail end of existing textile industry plants. This technology also shows promise for treating contaminated groundwaters, since pump-and-treat methods are an attractive pathway for remediating chlorinated solvents due to their relatively low retardation rate in water. For instance, the retardation rate of TCE is ~2, meaning that TCE migrates through aquifers at similar speeds to water (half speed since retardation rate = 2) and can therefore be removed from aquifers efficiently with pumping [1]. These advantages form a basis for how this technology might prove successful in treating these contaminants industrially in the future.

Appendix A: Supporting Information

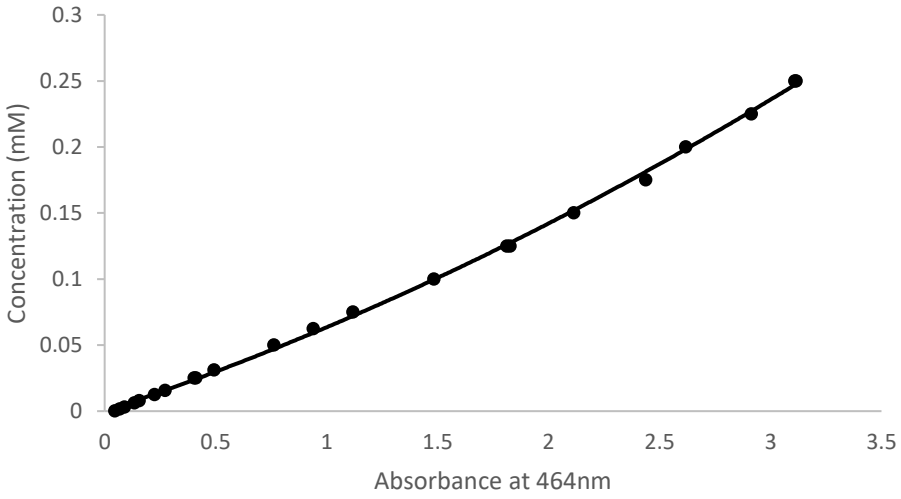

Figure S.1. A calibration curve generated for correlating absorbance of methyl orange samples at 464 nm to concentration (mM). The points represent stock solutions measured, while the line represents the result of a quadratic model determined with regression: $y = 0.0075x^2 + 0.056x$.

Repeated batch system experiments using nZVI-CNT Surface Composite Cathodes

In the series of batch system experiments using nZVI-CNT surface composite membranes at -2 V (discussed in Chapter 3), one of the membrane samples was used in a second test with identical parameters. This test was carried out to briefly examine whether repeatable values of MO batch removal could be achieved using the same nZVI-CNT membrane, anode, and applied voltage. The results of these two tests are displayed below in Figure S.2.

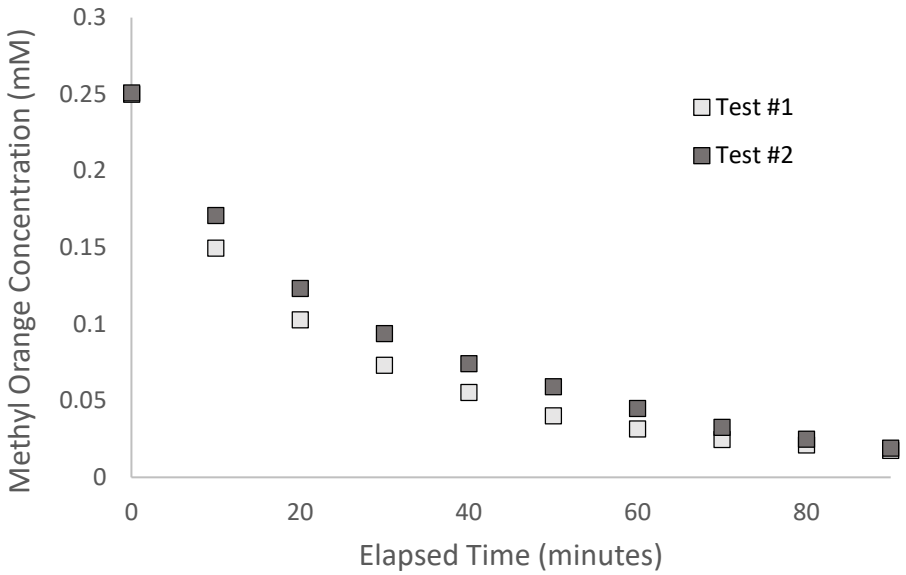

Figure S.2. Batch system results for a first (light) and second (dark) test run using an nZVI-CNT surface composite cathode and a graphite foil anode at -2 V.

The results shown in Figure S.2 suggest that the system in the second test is operating at a slightly reduced removal rate compared to the first experimental test. This slightly reduced performance could indicate that in successive runs of the batch removal system, sites for adsorption and reaction on the nZVI-CNT cathode are occupied by the products of the MO degradation reaction. However, given the size of the 95% confidence interval error bars in the data of the identical nZVI-CNT (-2 V) system shown in Figure 3.5, it is likely that the two series observed in Figure S.2 are within error of one another. Therefore, no definitive statistically significant claim can be made. More experiments are required to ascertain whether this phenomenon is occurring, and to thereby investigate how reusable this technology is.

Description of the custom continuous dead-end flow cell

The two-part cell is designed such that the top part screws down to clamp the membrane atop a porous support with an O-ring. The purpose of this configuration is such that the area of the membrane encompassed by the O-ring is exposed to the feed, while the area outside the O-ring is contacted by two stainless steel electrodes. The stainless-steel electrodes protrude from the flow cell, such that they can be attached to a voltage generator and conduct current to the surface of the membrane surface composite within.

Note that while the nitrogen gas cylinder was effective in applying a given pressure to the feed in the reservoir in which it was held, it is expected that the pressure of the flow just before the membrane surface is significantly reduced. This is due to the major and minor losses in fluid energy accrued through flow through system tubing, compressions and expansions in the flow path, changes in flow direction, and the exiting of flow from the system piping and into the main chamber of the dead end flow cell [144].

Measurement error in continuous experiments examining the effect of the mid-test application of voltage

It is likely that the MO permeate concentration reached steady state more rapidly than the data indicates. The results show that there is one sampling interval between the two steady states with permeate demonstrating intermediate MO removal (~68%), but this is likely because permeate leaving the membrane does not immediately exit the flow cell and into the permeate beaker, as it must first pass through the porous support on which the membrane sits, and then through a short channel. Thus, the value of mole % removed in the 30-40-minute interval reflects a mixture of MO permeate pre and post application of -2V voltage.

Table S.1. Data for 41 batch tests used to construct the PLSR model discussed in Chapter 5. Samples are coded according to the contents of their surface composites with the following convention: "CT" = nZVI-CNT, "T" = CNT, "S" = None.

Sample Name	Batch Concentration (mM)	Applied Voltage (V)	Electrode Spacing (cm)	nZVI Mass (mg)	CNT Mass (mg)	Surfactant Ratio (mg SDS: 1 mg CNTs)	Batch Volume (L)
CT25	0.25	-2	0.3	1.07	10	0	0.03
CT27	0.25	-2	0.3	1.07	10	0	0.03
CT28	0.25	-2	0.3	1.07	10	0	0.03
CT29	0.25	-2	0.3	1.07	10	0	0.03
CT30	0.25	-2	0.3	1.07	10	0	0.03
CT46	0.25	0	0.3	1.07	10	0	0.03
CT51	0.25	0	0.3	1.07	10	0	0.03
CT54	0.25	0	0.3	1.07	10	0	0.03
T7	0.25	-2	0.3	0	10	0	0.03
T8	0.25	-2	0.3	0	10	0	0.03
T9	0.25	-2	0.3	0	10	0	0.03
T6	0.25	-2	0.3	0	10	0	0.03
T13	0.25	0	0.3	0	10	0	0.03
T16	0.25	0	0.3	0	10	0	0.03
T18	0.25	0	0.3	0	10	0	0.03
CT62	0.025	-2	0.3	1.07	10	0	0.03
CT68	0.025	-2	0.3	1.07	10	0	0.03
CT55	0.025	-2	0.3	1.07	10	0	0.03
CT57	0.025	-2	0.3	1.07	10	0	0.03
CT??	0.025	0	0.3	1.07	10	0	0.03
CT??	0.025	0	0.3	1.07	10	0	0.03
CT??	0.025	-1	0.3	1.07	10	0	0.03
CT58	0.025	-1	0.3	1.07	10	0	0.03
CT63	0.025	-1	0.3	1.07	10	0	0.03
CT69	0.025	-1	0.3	1.07	10	0	0.03
CT67	0.025	-1	0.3	1.07	10	0	0.03
S1	0.025	-2	0.3	0	0	0	0.03
S2	0.025	0	0.3	0	0	0	0.03
CT125	0.025	-2	2	0.535	5	1	0.1
CT124	0.05	-1	1	0.535	5	1	0.1
CT108	0.025	-2	1	0.535	5	1.5	0.1
CT109	0.05	-1	2	0.535	5	1.5	0.1
CT106	0.05	-2	2	1.07	10	1.5	0.1
CT112	0.05	-2	1	1.07	10	1	0.1
CT103	0.025	-1	1	1.07	10	1.5	0.1
CT116	0.025	-1	2	1.07	10	1	0.1
CT121	0.025	0	1	1.07	10	1	0.1
CT117	0.05	0	1	1.07	10	1	0.1
T21	0.025	-2	1	0	10	1	0.1
T19	0.05	-2	1	0	10	1	0.1
T25	0.05	0	1	0	10	1	0.1

Appendix B: References

[1] H. H. Russell, J. E. Matthews, and G. W. Sewell, "Ground Water Issue: TCE Removal from Contaminated Soil and Ground Water," pp. 1–10, 1992.

[2] R. D. Fox, "Physical / Chemical Treatment of Organically Contaminated Soils and Sediments," *Air Waste Manag. Assoc.*, vol. 2247, 2012.

[3] H. Zollinger, *Color Chemistry: Syntheses, Properties, and Applications of Organic Dyes and Pigments*, Second Edi. Wiley-VCH Weinheim, 1991.

[4] K. Chung, "The significance of azo-reduction in the mutagenesis and carcinogenesis of azo dyes," vol. 114, pp. 269–281, 1983.

[5] H. Mansour, R. Mosrati, D. Corroler, K. Ghedira, D. Barillier, and L. Chekir, "In vitro mutagenicity of Acid Violet 7 and its degradation products by Pseudomonas putida mt-2 : Correlation with chemical structures," *Environ. Toxicol. Pharmacol.*, vol. 27, no. 2009, pp. 231–236, 2009.

[6] E. Engel, R. Vasold, and M. Landthaler, "Azo Pigments and a Basal Cell Carcinoma at the Thumb," 2008.

[7] J. Quinn, C. Geiger, C. Clausen, and K. Brooks, "Field Demonstration of DNAPL Dehalogenation Using Emulsified Zero-Valent Iron," *Environ. Sci. Technol.*, no. 519, pp. 1309–1318, 2005.

[8] V. K. Gupta, "Application of low-cost adsorbents for dye removal – A review," *J. Environ. Manage.*, vol. 90, no. 8, pp. 2313–2342, 2009.

[9] C. J. Geankoplis, *Transport Processes and Separation Process Principles*, 4th ed. Prentice

Hall PTR, 2011.

[10] J. a. Moulijn and A. Stankiewicz, "Process Intensification," *Chem. Eng. Prog.*, no. January, pp. 22–34, 2000.

[11] F. J. Armellini *et al.*, "Separations research needs for the 21st century," *Water Res.*, vol. 44, no. 3, pp. 283–288, 1992.

[12] E. Drioli and E. Fontananova, "Membrane technology and sustainable growth," *Chem. Eng. Res. Des.*, vol. 82, no. December, pp. 1557–1562, 2004.

[13] H. K. Lonsdale, "The Growth of Membrane Technology," *J. Memb. Sci.*, vol. 10, pp. 81–181, 1982.

[14] W. Guo, H. Ngo, and J. Li, "Bioresource Technology A mini-review on membrane fouling," *Bioresour. Technol.*, vol. 122, pp. 27–34, 2012.

[15] E. S. K. Chian and W. N. Bruce, "Removal of Pesticides by Reverse Osmosis," *Environ. Sci. Technol.*, no. 6, pp. 52–59, 1971.

[16] C. A. Buckley, "Membrane Technology for the Treatment of Dyehouse Effluents," *Water Sci. Technol.*, vol. 25, no. 10, pp. 203–209, 1992.

[17] D. De Jager, M. S. Sheldon, and W. Edwards, "Colour removal from textile wastewater using a pilot-scale dual-stage MBR and subsequent RO system," *Sep. Purif. Technol.*, vol. 135, pp. 135–144, 2014.

[18] N. Al-bastaki, "Removal of methyl orange dye and Na 2 SO 4 salt from synthetic waste water using reverse osmosis," *Chem. Eng. Process.*, vol. 43, pp. 1561–1567, 2004.

[19] C. Cripps, J. A. Bumpus, and S. D. Aust, "Biodegradation of Azo and Heterocyclic Dyes

by Phanerochaete chrysosporium," vol. 56, no. 4, pp. 1114–1118, 1990.

[20] T. Sale and C. Newell, "A Guide for Selecting Remedies for Subsurface Releases of Chlorinated Solvents," no. March. pp. 1–142, 2011.

[21] F. Obiri-Nyarko, S. J. Grajales-Mesa, and G. Malina, "An overview of permeable reactive barriers for in situ sustainable groundwater remediation," *Chemosphere*. 2014.

[22] L. Chen, S. Jin, P. H. Fallgren, N. G. Swoboda-Colberg, F. Liu, and P. J. S. Colberg, "Electrochemical depassivation of zero-valent iron for trichloroethene reduction," *J. Hazard. Mater.*, vol. 239–240, pp. 265–269, 2012.

[23] B. H. Kueper, H. F. Stroo, C. M. Vogel, and C. H. Ward, *Chlorinated Solvent Source Zone Remediation*. 2014.

[24] X. Guan *et al.*, "The limitations of applying zero-valent iron technology in contaminants sequestration and the corresponding countermeasures: The development in zero-valent iron technology in the last two decades (1994-2014)," *Water Res.*, vol. 75, pp. 224–248, 2015.

[25] Y. Liu, T. Phenrat, and G. V. Lowry, "Effect of TCE concentration and dissolved groundwater solutes on NZVI-promoted TCE dechlorination and H2 evolution," *Environ. Sci. Technol.*, vol. 41, no. 22, pp. 7881–7887, 2007.

[26] F. Fu, D. D. Dionysiou, and H. Liu, "The use of zero-valent iron for groundwater remediation and wastewater treatment: A review," *J. Hazard. Mater.*, vol. 267, pp. 194–205, 2014.

[27] T. Phenrat, T. Thongboot, and G. V. Lowry, "Electromagnetic Induction of Zerovalent Iron (ZVI) Powder and Nanoscale Zerovalent Iron (NZVI) Particles Enhances Dechlorination of

Trichloroethylene in Contaminated Groundwater and Soil: Proof of Concept," *Environ. Sci. Technol.*, vol. 50, no. 2, pp. 872–880, 2016.

[28] Z. Zongshan, L. I. U. Jingfu, T. A. I. Chao, Z. Qunfang, H. U. Jingtian, and J. Guibin, "Rapid decolorization of water soluble azo-dyes by nanosized zero-valent iron immobilized on the exchange resin," *Sci. China Ser. B Chem.*, vol. 51, no. 20537020, 2008.

[29] S. Nam and P. G. T. M, "Reduction of Azo Dyes with Zero-Valent Iron," vol. 34, no. 6, pp. 1837–1845, 2000.

[30] I. Mcdonald *et al.*, "Rusty old stars: a source of the missing interstellar iron?," 2018.

[31] X. Lv *et al.*, "Nanoscale Zero-Valent Iron (nZVI) assembled on magnetic Fe3O4/graphene for Chromium (VI) removal from aqueous solution," *J. Colloid Interface Sci.*, vol. 417, pp. 51–59, 2014.

[32] X. Zhao, W. Liu, Z. Cai, B. Han, T. Qian, and D. Zhao, "An overview of preparation and applications of stabilized zero-valent iron nanoparticles for soil and groundwater remediation," *Water Res.*, vol. 100, pp. 245–266, 2016.

[33] W. Zhang, C. Wang, and H. Lien, "Treatment of chlorinated organic contaminants with nanoscale bimetallic particles," vol. 40, pp. 387–395, 1998.

[34] Y. Sun, J. Li, T. Huang, and X. Guan, "The influences of iron characteristics, operating conditions and solution chemistry on contaminants removal by zero-valent iron: A review," *Water Res.*, vol. 100, pp. 277–295, 2016.

[35] J. Fan, Y. Guo, J. Wang, and M. Fan, "Rapid decolorization of azo dye methyl orange in aqueous solution by nanoscale zerovalent iron particles," *J. Hazard. Mater.*, vol. 166, pp.

904–910, 2009.

[36] R. A. Crane and T. B. Scott, “Nanoscale zero-valent iron : Future prospects for an emerging water treatment technology,” *J. Hazard. Mater.*, vol. 211–212, pp. 112–125, 2012.

[37] Q. Wang, H. Qian, Y. Yang, Z. Zhang, C. Naman, and X. Xu, “Reduction of hexavalent chromium by carboxymethyl cellulose-stabilized zero-valent iron nanoparticles,” *J. Contam. Hydrol.*, vol. 114, no. 1–4, pp. 35–42, 2010.

[38] N. C. Mueller *et al.*, “Application of nanoscale zero valent iron (NZVI) for groundwater remediation in Europe,” *Environ. Sci. Pollut. Res.*, vol. 19, no. 2, pp. 550–558, 2012.

[39] C. F. de Lannoy, D. Jassby, D. D. Davis, and M. R. Wiesner, “A highly electrically conductive polymer-multiwalled carbon nanotube nanocomposite membrane,” *J. Memb. Sci.*, vol. 415–416, pp. 718–724, 2012.

[40] M. Oner, O. Dogan, and G. Oner, “The influence of polyelectrolytes architecture on calcium sulfate dihydrate growth retardation,” *J. Cryst. Growth*, vol. 186, pp. 427–437, 1998.

[41] K. H. Schoenbach, F. E. Peterkin, R. W. Alden, and S. J. Beebe, “The Effect of Pulsed Electric Fields on Biological Cells : Experiments and Applications,” *IEEE Trans. Plasma Sci.*, vol. 25, no. 2, pp. 284–292, 1997.

[42] O. Paper, “Electrochemical prevention of marine biofouling on a novel titanium-nitride-coated plate formed by radio-frequency arc spraying,” *Appl. Microbiol Biotechnol*, pp. 502–509, 1998.

[43] S. Shim, S. H. Hong, Y. Tak, and J. Yoon, “Prevention of Pseudomonas aeruginosa adhesion by electric currents,” *Biofouling*, vol. 7014, 2011.

[44] U. R. Farooqui, A. L. Ahmad, and N. A. Hamid, “Graphene oxide : A promising membrane material for fuel cells,” *Renew. Sustain. Energy Rev.*, vol. 82, no. July 2017, pp. 714–733, 2018.

[45] F. Perreault, A. Fonseca de Faria, and M. Elimelech, “Environmental applications of graphene-based nanomaterials,” *Chem. Soc. Rev.*, vol. 44, no. 16, pp. 5861–5896, 2015.

[46] Z. Li, L. Wang, L. Yuan, C. Xiao, L. Mei, and L. Zheng, “Efficient removal of uranium from aqueous solution by zero-valent iron nanoparticle and its graphene composite,” *J. Hazard. Mater.*, vol. 290, pp. 26–33, 2015.

[47] H. Chen, Y. Cao, E. Wei, T. Gong, and Q. Xian, “Chemosphere Facile synthesis of graphene nano zero-valent iron composites and their ef fi cient removal of trichloronitromethane from drinking water,” *Chemosphere*, vol. 146, pp. 32–39, 2016.

[48] P. Geladi, “Notes on the History and Nature of Partial Least Squares (PLS) Modelling,” vol. 2, no. October 1987, pp. 231–246, 1988.

[49] A. Moores and M. Kauhsik, “Review - nanocellulose as versatile supports for metal nanoparticles and their applications in catalysis,” *Green Chem.*, pp. 622–637, 2016.

[50] T. Pradeep, “Noble metal nanoparticles for water purification : A critical review,” *Thin Solid Films*, vol. 517, no. 24, pp. 6441–6478, 2009.

[51] S. Y. Yang, C. D. Vecitis, and H. Park, “Electrocatalytic water treatment using carbon nanotube filters modified with metal oxides,” *Environ. Sci. Pollut. Res.*, pp. 1–8, 2017.

[52] C. D. Vecitis, G. Gao, and H. Liu, “Electrochemical carbon nanotube filter for adsorption, desorption, and oxidation of aqueous dyes and anions,” *J. Phys. Chem. C*, vol. 115, no. 9,

pp. 3621–3629, 2011.

[53] B. Huang, C. Lei, C. Wei, and G. Zeng, “Chlorinated volatile organic compounds (Cl-VOCs) in environment — sources , potential human health impacts , and current remediation technologies,” *Environ. Int.*, vol. 71, pp. 118–138, 2014.

[54] R. Sengupta *et al.*, “A Short Review on Rubber / Clay Nanocomposites With Emphasis on Mechanical Properties,” *Engineering*, vol. 47, pp. 21–25, 2007.

[55] P. K. Tandon, R. C. Shukla, and S. B. Singh, “Removal of Arsenic (III) from Water with Clay-Supported Zerovalent Iron Nanoparticles Synthesized with the Help of Tea Liquor,” no. Iii, 2013.

[56] A. D. Towns, “Developments in azo disperse dyes derived from heterocyclic diazo components,” vol. 42, 1999.

[57] A. Tilche and D. Orhon, “Appropriate basis of effluent standards for industrial wastewaters,” *Water Sci. Technol.*, vol. 45, no. 12, pp. 1–12, 2002.

[58] S. N. Petrova, M. V. Volodarskii, S. V. Makarov, and L. Z. Li, “Oxidation of Azo Dyes with Inorganic Peroxides in the Presence of Cationic Surfaces,” *Russ. J. Appl. Chem.*, vol. 81, no. 9, pp. 1573–1577, 2008.

[59] T. Robinson, G. Mcmullan, R. Marchant, and P. Nigam, “Remediation of dyes in textile effluent : a critical review on current treatment technologies with a proposed alternative,” *Bioresour. Technol.*, vol. 77, pp. 247–255, 2001.

[60] E. Brillas and C. A. Martinez-Huitle, “Applied Catalysis B : Environmental Decontamination of wastewaters containing synthetic organic dyes by electrochemical

methods : A general review," *Appl. Catal. B Environ.*, vol. 87, pp. 105–145, 2009.

[61] I. M. Banat, P. Nigam, D. Singh, and R. Marchant, "Microbial Decolorization of Textile-Dye Containing Effluents: A Review," vol. 58, no. 1996, pp. 217–227, 1997.

[62] W. Chou, C. Wang, and C. Chang, "Comparison of removal of Acid Orange 7 by electrooxidation using various anode materials," *Desalination*, vol. 266, no. 1–3, pp. 201–207, 2011.

[63] E. Guivarch, S. Trevin, and C. Lahitte, "Degradation of azo dyes in water by Electro-Fenton process," *Env. Chem Lett*, pp. 38–44, 2003.

[64] V. Perazzolo, C. Durante, and A. Gennaro, "Nitrogen and sulfur doped mesoporous carbon cathodes for water treatment," *J. Electroanal. Chem.*, vol. 782, pp. 264–269, 2016.

[65] D. Pant, A. Singh, G. Van Bogaert, I. Olsen, and S. Nigam, "Bioelectrochemical systems (BES) for sustainable energy production and product recovery from organic wastes and industrial wastewaters," *RSC Adv.*, pp. 1248–1263, 2012.

[66] K. C. L. N. Rao, K. Krishnaiah, and Ashutosh, "Colour Removal from a Dyestuff Industry Effluent Using Activated Carbon," *Indian J. Chem. Technol.*, no. January, pp. 13–19, 1994.

[67] D. González, J. Amigo, and F. Suárez, "Membrane distillation : Perspectives for sustainable and improved desalination," *Renew. Sustain. Energy Rev.*, vol. 80, no. April 2016, pp. 238–259, 2017.

[68] N. Voutchkov, "Energy use for membrane seawater desalination – current status and trends," *Desalination*, vol. 431, no. October 2017, pp. 2–14, 2018.

[69] A. W. Mohammad and C. Y. Ng, "Ultrafiltration in Food Processing Industry : Review on

Application , Membrane Fouling , and Fouling Control," *Food Bioprocess Technol*, pp. 1143–1156, 2012.

[70] A. Deshmukh *et al.*, "Environmental Science Membrane distillation at the water-energy nexus : limits , opportunities , and challenges," *Energy Environ. Sci.*, vol. 11, pp. 1177–1196, 2018.

[71] B. Van Der Bruggen, C. Vandecasteele, T. Van Gestel, W. Doyenb, and R. Leysenb, "Review of Pressure-Driven Membrane Processes," *Environ. Prog.*, vol. 22, no. 1, pp. 46–56, 2003.

[72] M. Rezakazemi and A. Ebadi, "Progress in Polymer Science State-of-the-art membrane based CO 2 separation using mixed matrix membranes (MMMs): An overview on current status and future directions," *Prog. Polym. Sci.*, vol. 39, no. 5, pp. 817–861, 2014.

[73] W. Gao *et al.*, "Membrane fouling control in ultra fi ltration technology for drinking water production : A review," *Desalination*, vol. 272, no. 1–3, pp. 1–8, 2011.

[74] "Rosmosis Ltd.," 2009. [Online]. Available: http://www.rosmosis.com/page.aspx?page_id=78.

[75] Y. Tanaka, S. Moon, V. V Nikonenko, and T. Xu, "Ion-Exchange Membranes," *Int. J. Chem. Eng.*, vol. 2012, 2012.

[76] B. Singh, V. Kochkodan, R. Hashaikeh, and N. Hilal, "A review on membrane fabrication : Structure , properties and performance relationship," *Desalination*, vol. 326, pp. 77–95, 2013.

[77] M. Elimelech, "Organic Fouling and Chemical Cleaning of Nanofiltration Membranes :

Measurements and Mechanisms," *Environ. Sci. Technol.*, vol. 38, no. 17, pp. 4683–4693, 2004.

[78] P. Watnick, "MINIREVIEW Biofilm , City of Microbes," *J. Bacteriol.*, vol. 182, no. 10, pp. 2675–2679, 2000.

[79] R. M. Donlan, "Biofilms: Microbial Life on Surfaces," *Emerg. Infect. Dis.*, vol. 8, no. 9, pp. 881–890, 2002.

[80] N. Hilal *et al.*, "Methods Employed for Control of Fouling in MF and UF Membranes : A Comprehensive Review," *Sep. Sci. Technol.*, vol. 6395, 2007.

[81] G. Amy, "Fundamental understanding of organic matter fouling of membranes," *Desalination*, vol. 231, pp. 44–51, 2008.

[82] R. D. Cohen and R. F. Probstein, "Colloidal Fouling of Reverse Osmosis Membranes," *J. Colloid Interface Sci.*, vol. 114, no. 1, pp. 194–207, 1986.

[83] G. B. T, R. H. Davis, and A. L. Zydney, "The behavior of suspensions and macromolecular solutions in crossflow microfiltration," *J. Memb. Sci.*, vol. 96, pp. 1–58, 1994.

[84] E. S. P. B. V, M. Bruslovsky, and J. Borden, "Flux decline due to gypsum precipitation on RO membranes," *Desalination*, vol. 86, pp. 187–222, 1992.

[85] C. Tzotzi, T. Pahiadaki, S. G. Yiantsios, A. J. Karabelas, and N. Andritsos, "A study of CaCO 3 scale formation and inhibition in RO and NF membrane processes," *J. Memb. Sci.*, vol. 296, pp. 171–184, 2007.

[86] R. Klaassen, P. H. M. Feron, and A. E. Jansen, "Membrane Contactors in Industrial Applications," *Chem. Eng. Res. Des.*, vol. 83, no. March, pp. 234–246, 2005.

[87] R. Klaassen and A. E. Jansen, “The Membrane Contactor : Environmental Applications and Possibilities,” *Environ. Prog.*, vol. 20, no. 1, pp. 37–43, 2001.

[88] S. Schlosser, “Separation of mixtures by pertraction or membrane based solvent extraction and new extractants,” no. January 2009, 2014.

[89] S. Mozia, M. Tomaszewska, and A. W. Morawski, “Photocatalytic membrane reactor (PMR) coupling photocatalysis and membrane distillation — Effectiveness of removal of three azo dyes from water,” *Catal. Today*, vol. 129, pp. 3–8, 2007.

[90] S. Mozia, M. Tomaszewska, and A. W. Morawski, “A new photocatalytic membrane reactor (PMR) for removal of azo-dye Acid Red 18 from water,” *Appl. Catal. B Environ.*, vol. 59, pp. 131–137, 2005.

[91] E. Alventosa-deLara, S. Barredo-Damas, M. I. Alcaina-Miranda, and M. I. Iborra-Clar, “Ultrafiltration technology with a ceramic membrane for reactive dye removal : Optimization of membrane performance,” *J. Hazard. Mater.*, vol. 209–210, pp. 492–500, 2012.

[92] F. Ibney, K. Yamamoto, F. Nakajima, and K. Fukushi, “Removal of structurally different dyes in submerged membrane fungi reactor — Biosorption / PAC-adsorption , membrane retention and biodegradation,” *J. Memb. Sci.*, vol. 325, pp. 395–403, 2008.

[93] A. Ronen, W. Duan, I. Wheeldon, S. Walker, and D. Jassby, “Microbial Attachment Inhibition through Low-Voltage Electrochemical Reactions on Electrically Conducting Membranes,” *Environ. Sci. Technol.*, 2015.

[94] C. F. De Lannoy, D. Jassby, K. Gloe, A. D. Gordon, and M. R. Wiesner, “Aquatic biofouling

prevention by electrically charged nanocomposite polymer thin film membranes," *Environ. Sci. Technol.*, vol. 47, no. 6, pp. 2760–2768, 2013.

[95] B. P. Chaplin, "Critical Review of Electrochemical Advanced Oxidation Processes for Water Treatment Applications," *Environ. Sci. Process Impacts*, pp. 1–23, 2012.

[96] E. S. P. B. V, S. Avlonitis, and T. Hodgkiess, "Chlorine Degradation of Aromatic Polyamides," *Desalination*, vol. 5, no. 85, pp. 321–334, 1992.

[97] C. D. Vecitis, "Electrochemical Carbon Nanotube Filter Oxidative Performance as a Function of Surface Chemistry Electrochemical Carbon Nanotube Filter Oxidative Performance as a Function of Surface Chemistry," *Environ. Sci. Technol.*, pp. 9726–9734, 2011.

[98] W. Duan, G. Chen, C. Chen, R. Sanghvi, A. Iddya, and S. Walker, "Electrochemical removal of hexavalent chromium using electrically conducting carbon nanotube / polymer composite ultra filtration membranes," *J. Memb. Sci.*, vol. 531, no. March, pp. 160–171, 2017.

[99] L. C. Venema, J. W. G. Wildo, and C. Dekker, "Electronic structure of atomically resolved carbon nanotubes ¨," *Nature*, vol. 584, no. 10, pp. 1996–1999, 1998.

[100] Y. Liu and G. V. Lowry, "Effect of particle age (Fe0 content) and solution pH on NZVI reactivity: H2 evolution and TCE dechlorination," *Environ. Sci. Technol.*, vol. 40, no. 19, pp. 6085–6090, 2006.

[101] L. Yong, A. Wahab, C. Peng, and N. Hilal, "Polymeric membranes incorporated with metal / metal oxide nanoparticles : A comprehensive review Polymeric membranes incorporated

with metal / metal oxide nanoparticles : A comprehensive review," *Desalination*, vol. 308, no. January, pp. 15–33, 2010.

[102] R. Mukherjee, R. Kumar, A. Sinha, Y. Lama, and A. Krishna, "Technology A review on synthesis , characterization , and applications of nano zero valent iron (nZVI) for environmental remediation," *Crit. Rev. Environ. Sci. Technol.*, vol. 46, no. 5, pp. 443–466, 2016.

[103] S. Li, W. Yan, and W. Zhang, "Solvent-free production of nanoscale zero-valent iron (nZVI) with precision milling," *Green Chem.*, pp. 1618–1626, 2009.

[104] F. He and D. Zhao, "Manipulating the Size and Dispersibility of Zerovalent Iron Nanoparticles by Use of Carboxymethyl Cellulose Stabilizers," *Environ. Sci. Technol.*, vol. 41, no. 17, pp. 6216–6221, 2007.

[105] N. T. K. Thanh, N. Maclean, and S. Mahiddine, "Mechanisms of Nucleation and Growth of Nanoparticles in Solution," *Chem. Rev.*, vol. 3, no. 1, 2014.

[106] P. Kanuparthi, *Phytotoxicity of Nanoparticles*, no. June 2018. 2019.

[107] T. Phenrat and N. Saleh, "Aggregation and Sedimentation of Aqueous Nanoscale Zerovalent Iron Dispersions," *Environ. Sci. Technol.*, vol. 41, no. 1, pp. 284–290, 2007.

[108] F. He, D. Zhao, J. Liu, and C. B. Roberts, "Stabilization of Fe - Pd Nanoparticles with Sodium Carboxymethyl Cellulose for Enhanced Transport and Dechlorination of Trichloroethylene in Soil and Groundwater," *Ind. Eng. Chem. Res.*, vol. 46, pp. 29–34, 2007.

[109] B. Chisholm, "Polymer modified iron nanoparticles for environmental remediation,"

Polym. Prepr., no. January 2008, pp. 3–5, 2015.

[110] A. Tiraferri and Æ. R. Sethi, "Enhanced transport of zerovalent iron nanoparticles in saturated porous media by guar gum," *J. Nanoparticle Res.*, pp. 635–645, 2009.

[111] A. Tiraferri, K. Loon, R. Sethi, and M. Elimelech, "Journal of Colloid and Interface Science Reduced aggregation and sedimentation of zero-valent iron nanoparticles in the presence of guar gum," *J. Colloid Interface Sci.*, vol. 324, pp. 71–79, 2008.

[112] N. Saleh *et al.*, "Adsorbed Triblock Copolymers Deliver Reactive Iron Nanoparticles to the Oil / Water Interface," *Nano Lett.*, vol. 5, no. 12, pp. 2489–2494, 2005.

[113] A. N. Bezbaruah, S. Krajangpan, B. J. Chisholm, E. Khan, and J. J. Elorza, "Entrapment of iron nanoparticles in calcium alginate beads for groundwater remediation applications," *J. Hazard. Mater.*, vol. 166, pp. 1339–1343, 2009.

[114] N. Saleh *et al.*, "Surface Modifications Enhance Nanoiron Transport and NAPL Targeting in Saturated Porous Media," *Environ. Eng. Sci.*, vol. 24, no. 1, 2007.

[115] N. Saleh and H. Kim, "Ionic Strength and Composition Affect the Mobility of in Water-Saturated Sand Columns," *Environ. Sci. Technol.*, pp. 3349–3355, 2008.

[116] S. Raj and K. Æ. Dhriti, "Transport of surface-modified iron nanoparticle in porous media and application to arsenic (III) remediation," *J. Nanoparticle Res.*, pp. 725–735, 2007.

[117] B. W. Hydutsky, E. J. Mack, B. B. Beckerman, J. M. Skluzacek, and T. E. Mallouk, "Optimization of Nano- and Microiron Transport through Sand Columns Using Polyelectrolyte Mixtures," *Environ. Sci. Technol.*, vol. 41, no. 18, pp. 6418–6424, 2007.

[118] K. M. Sirk, N. B. Saleh, T. Phenrat, H. Kim, B. Dufour, and J. Ok, "Effect of Adsorbed

Polyelectrolytes on Nanoscale Zero Valent Iron Particle Attachment to Soil Surface Models," *Environ. Sci. Technol.*, vol. 43, no. 10, pp. 3803–3808, 2009.

[119] S. R. Kanel and H. Choi, "Transport characteristics of surface-modified nanoscale zero-valent iron in porous media," *Water Sci. Technol.*, vol. 55, no. 1–2, pp. 157–162, 2007.

[120] B. Zhu and T. Lim, "Influences of Amphiphiles on Dechlorination of a Trichlorobenzene by Nanoscale Pd / Fe : Adsorption , Reaction Kinetics , and Interfacial Interactions," *Environ. Sci. Technol.*, vol. 42, no. 12, pp. 4513–4519, 2008.

[121] L. I. Xie and C. Shang, "Role of Humic Acid and Quinone Model Compounds in Bromate Reduction by Zerovalent Iron," *Environ. Sci. Technol.*, vol. 39, no. 4, pp. 1092–1100, 2005.

[122] B. Zhu, T. Lim, and J. Feng, "with palladized nanoscale Fe 0 particles supported on chitosan and silica," *Chemosphere*, vol. 65, pp. 1137–1145, 2006.

[123] B. Geng, Z. Jin, T. Li, and X. Qi, "Chemosphere Kinetics of hexavalent chromium removal from water by chitosan-Fe 0 nanoparticles," *Chemosphere*, vol. 75, no. 6, pp. 825–830, 2009.

[124] H. C. Choi, M. Shim, S. Bangsaruntip, H. Dai, and S. U. V, "Spontaneous Reduction of Metal Ions on the Sidewalls of Carbon Nanotubes," pp. 9058–9059, 2002.

[125] B. Kim, W. M. Sigmund, and P. O. Box, "Functionalized Multiwall Carbon Nanotube / Gold Nanoparticle Composites," no. 17, pp. 8239–8242, 2004.

[126] J. Yang, X. Liu, L. Huang, and D. Sun, "Antibacterial Properties of Novel Bacterial Cellulose Nanofiber," *Chinese J. Chem. Eng.*, vol. 21, no. 12, pp. 1419–1424, 2013.

[127] E. Petala, K. Dimos, A. Douvalis, T. Bakas, and J. Tucek, "Nanoscale zero-valent iron

supported on mesoporous silica : Characterization and reactivity for Cr (VI) removal from aqueous solution," *J. Hazard. Mater.*, vol. 261, pp. 295–306, 2013.

[128] X. Qiu, Z. Fang, B. Liang, F. Gu, and Z. Xu, "Degradation of decabromodiphenyl ether by nano zero-valent iron immobilized in mesoporous silica microspheres," *J. Hazard. Mater.*, vol. 193, pp. 70–81, 2011.

[129] P. D. Mines *et al.*, "Granular activated carbon with grafted nanoporous polymer enhances nanoscale zero-valent iron impregnation and water contaminant removal," *Chem. Eng. J.*, vol. 339, no. January, pp. 22–31, 2018.

[130] H. Dong, J. Deng, Y. Xie, C. Zhang, and Z. Jiang, "Stabilization of nanoscale zero-valent iron (nZVI) with modified biochar for Cr (VI) removal from aqueous solution," *J. Hazard. Mater.*, vol. 332, pp. 79–86, 2017.

[131] J. Isrealachvili, *Intermolecular and Surface Forces*, Third. Elsevier, 2011.

[132] M. Zarei, A. R. Khataee, and M. Fathinia, "Electrochimica Acta Photoelectro-Fenton combined with photocatalytic process for degradation of an azo dye using supported TiO 2 nanoparticles and carbon nanotube cathode : Neural network modeling," *Electrochim. Acta*, vol. 55, no. 24, pp. 7259–7265, 2010.

[133] M. A. Halali, "The Effect of Cross-Linkers on the Permeability of Electrically Conductive Membranes," *Ind. Eng. Chem. Res.*, 2019.

[134] D. A. Y. M. Scholz, *Textile dye wastewater characteristics and constituents of synthetic effluents : a critical review*, vol. 16, no. 2. Springer Berlin Heidelberg, 2018.

[135] G. Gao, Z. Qiaoying, and C. Vecitis, "CNT–PVDF composite flow-through electrode for

single-pass sequential reduction–oxidation," *J. Mater. Chem. A*, no. 2, pp. 6185–6190, 2014.

[136] A. Sweity, Y. Oren, Z. Ronen, and M. Herzberg, "The influence of antiscalants on biofouling of RO membranes in seawater desalination," *Water Res.*, vol. 47, no. 10, pp. 3389–3398, 2013.

[137] T. E. Marlin, "Process Control," 2007.

[138] F. Mugele and J.-Ch. Baret, "Electrowetting : from basics to applications," *J. Phys. Condens. Matter*, 2005.

[139] S. Wold and M. Sjostrom, "PLS-regression : a basic tool of chemometrics," pp. 109–130, 2001.

[140] J. V Kresta, J. F. Macgregor, and T. E. Marlin, "Multivariate Statistical Monitoring of Process Operating Performance," vol. 69, 1991.

[141] C. Wikstrom, E. Johansson, A. Nordahl, S. Rannar, and M. Sandberg, "Multivariate process and quality monitoring applied to an electrolysis process Part II . Multivariate time-series analysis of lagged latent variables," pp. 233–240, 1998.

[142] J. M. Campos-martin, G. Blanco-brieva, and J. L. G. Fierro, "Hydrogen Peroxide Synthesis : An Outlook beyond the Anthraquinone Process Angewandte," pp. 6962–6984, 2006.

[143] Y. Liu, Q. Fan, Y. Liu, and J. Wang, "Fenton-like oxidation of 4-chlorophenol using H 2 O 2 in situ generated by Zn-Fe-CNTs composite," *J. Environ. Manage.*, vol. 214, pp. 252–260, 2018.

[144] P. J. Pritchard and J. W. Mitchell, *Fox and McDonald's Introduction to Fluid Mechanics*,

9th ed. Wiley & Sons, 2015.